Article

Not peer-reviewed version

Hydrodynamic Similarity of Different Power Levels and Dynamic Analysis of Ocean Current Converter-Platform Systems with a Novel Pulley-Traction Rope Design under Typhoon Irregular Wave and Current

Shueei-Muh Lin *, Wen-Rong Wang , Hsin Yuan

Posted Date: 24 July 2024

doi: 10.20944/preprints202407.1940.v1

Keywords: similarity law; MW convertor; stability; dynamic tension; ocean current; hydrodynamic damping; translational displacement; rotational displacement; pulley-traction rope design; platform; pontoon; two foundations

Article

Hydrodynamic Similarity of Different Power Levels and Dynamic Analysis of Ocean Current Converter-Platform Systems with a Novel Pulley-Traction Rope Design under Typhoon Irregular Wave and Current

Shueei-Muh Lin *, Wen-Rong Wang and Hsin Yuan

Green Energy Technology Research Centre (GETRC), Department of Mechanical Engineering, Kun Shan University, Tainan 710, Taiwan; me70ks10@mail.ksu.edu.tw (W.-R.W.); qeye@yahoo.com.tw (H.Y.)
* Correspondence: smlin45@gmail.com

Abstract: In the future, the power of commercial ocean current generators can reach MW level, and the corresponding mooring rope tension is very great. But the power of the ocean current generator in research stage is KW level and it can bear less rope tension. Its main mooring rope adopts a single cable and a single foundation. This paper studies the dynamic response and rope tension of the MW-level ocean current generator mooring system. It is assumed that the commercial MW-level ocean current generator is similar to the research-type KW level, and the similarity law and several dimensionless similar parameters are proposed, including for the turbine and platform the power number, tip speed ratio, hydrodynamic damping and stiffness coefficient and others. Based on these dimensionless similar formulas and the known parameters of the researched KW-level convertor, all parameters of the MW-level ocean current generator are derived. In order to overcome the extreme tension of a MW-level mooring system and provide good stability, this paper proposes the pulley-traction rope design to replace the traditional single traction rope design. The static and dynamic mathematical models of this mooring system subjected to typhoon wave impact and current are proposed and analytical solutions are obtained. The study found that the dynamic rope tension of the MW-level system with the traditional single rope system is significantly greater than its fracture strength and the dynamic tension of the pulley- traction rope system. It means that this design can effectively reduce the dynamic rope tensions of the mooring system. Moreover, if the length ratio of rope A to the seabed depth is within a safe range, the maximum rope dynamic tension will be less than the fracture strength. In addition to the MW level, the dynamic response of the 700kW level power generation system under the action of typhoon waves is also studied. It is discovered that the dynamic tension of rope D is the largest. In addition, the dynamic tension of rope D for 700kW system will exceed the original strength of design. However, only the specification of rope D is increased, the new dynamic tension is still close to the original such that the dynamic tension of rope D is significantly less than the adjusted fracture strength and the mooring system becomes safety.

Keywords: similarity law; MW convertor; stability; dynamic tension; ocean current; hydrodynamic damping; translational displacement; rotational displacement; pulley- traction rope design; platform; pontoon; two foundations

1. Introduction

Global ocean currents are rich in energy. The potential electricity capacity in the Taiwan Kuroshio current is over 4GW [1]. The core technologies of ocean current power generation are being investigated [1–5]. The relevant technologies include (1) the high-efficiency convertor, (2) the deep

 doi:10.20944/preprints202407.1940.v1

mooring technology for over 1000m depth seabed beneath the current, (3) the protection from the typhoon wave impact, (4) double main traction ropes for high power convertor, and (5) the investigation of the mathematical model with the fluid-structure interaction (FSI).

WanChi company developed a 50 kW ocean current convertor which the blade is pushed by the current force and moved in the translational motion. Chen *et al*. [1] successfully tested the 50 kW WanChi convertor moored to the 850 m deep seabed beneath Kuroshio current at Taiwan Pingtung sea area. IHI and NEDO [2] developed a 100 kW ocean current convertor which was integrated by two sets of rotational turbines. The 100kW convertor was successfully tested by mooring to the 100 m deep seabed beneath the Japan Kuroshio current. Guo *et al*. [3] developed a 20 kW ocean current convertor which was integrated by two sets of rotational turbines. The 20kW convertor was tested by mooring it to the 80 m deep seabed beneath the Taiwan Liuqiu sea area.

The deep mooring theory and technology for the ocean current convertor system are important. A few of literatures investigated the dynamic stability of this mooring system under the coupled current-wave effect. WanChi company further developed a 400 kW ocean current convertor following the principle of the 50 kW ones. Lin *et al*. [4] proposed the mathematical model of the 400 kW ocean convertor-pontoon-traction rope-foundation mooring system under the coupled regular wave-ocean current effects. The motion of this system is four degrees of freedom. The dynamic system include the heaving motion of pontoon and the coupled surging-heaving-pitching motion of the convertor. The dynamic performance and stability of the system under coupled wave-current effect were investigated. Lin and Chen [5] proposed a towed parachute-platform-traction rope-foundation mooring system which protected the submarined platform from the typhoon wave impact. The concentrated mass model was considered. The motion of this system was three degrees of freedom. The coupled motions included surging and heaving of elements. It was theoretically verified the protection function of the proposed methodology under Typhoon wave impact. Lin *et al*. [6] presented the submarined ocean convertor-surfaced platform-pontoon-traction rope-foundation mooring system. The concentrated mass model was considered. The motion of this system was five degrees of freedom. The coupled motion included surging and heaving of elements. The dynamic stability of the mooring system under the regular wave and steady ocean current was investigated. Lin *et al*. [7] presented the submarined ocean convertor-submarined platform-2 pontoon-traction rop-foundation mooring system. The concentrated mass model was considered. The motion of this system was six degrees of freedom. The coupled motion included surging and heaving of elements. The dynamic response of this mooring system under the typhoon irregular wave of at Taiwan's Green Island during the 50-year regression period was investigated. Lin *et al.* [8] designed a 400kW convertor composed of two rotating horizontal turbines. The hydrodynamic damping and stiffness coefficients were determined by using the computational fluid method. The submarined 400kW convertor-submarined platform-2 pontoon-traction rop-foundation mooring system was considered. The motion of this system was eighteen degrees of freedom. The coupled 3D motion included the translational and rotational of elements. The frequency spectrum of the system with the coupled fluid-structure interaction and regular wave was studied. Further, Lin *et al*. [9] investigated the transient performance of the 18 DOF mooring system with inital conditions. Pierson and Moskowitz [10] proposed the Jonswap spectrum and confirmed it with experimental measurement results. To simplify actual irregular ocean waves, a limited number of regular wave are usually used to approximate the irregular wave [7]. This study will take several regular waves to simulate irregular waves according to the experimental significant wave height, frequency and the Jonswap wave spectrum. In the literatures [4–9], the mooring traction rope is single only. However, for high power convertor its traction force is very great, two traction ropes is necessary. The relavant investgation is helpful for the ocean energy technology.

Theorem and technology of fluid structure interaction (FSI) are widely applied in many different fields including marine engineering [11,12], aerodynamics [13], acoustics [14] and biomechanics [15]. Due to the complexity of the fluid-structure interaction, a few literatures investigated the FSI problem by using analytical method [15], but mostly the numerical methods: (1) the boundary element method [13], (2) the finite-volume method [16], (3) the Coupled SPH–FEM [17].

Preprints.org (www.preprints.org) | NOT PEER-REVIEWED | Posted: 24 July 2024 doi:10.20944/preprints202407.1940.v1

So far, the relative literatures proposed one single main mooring rope connecting to one foundation. For the high-power ocean current convertor, this study designs a pulley-traction rope set which the rope connects to the two foundations. The similarity law is proposed to calculate the hydrodynamic damping and stiffness coefficient of turbine and platform. The static and dynamic equations of this ocean current power generation anchoring system are proposed to study the rope tension and stability under irregular waves.

2. Mathematical Model

To avoid the wave impact of typhoons, the energy convertor and the floating platform were submerged to a safe depth. For safely mooring a high power ocean convertor this study presents a pulley- traction rope set composed of a pulley and one main rope connected to two separate foundations, as shown in Figure 1. The coupled translational-rotational motion of the mooring system under coupled wave-current effect are considered. The motion is eighteen degrees of freedom. The governing equations of this mooring system are derived as follows:

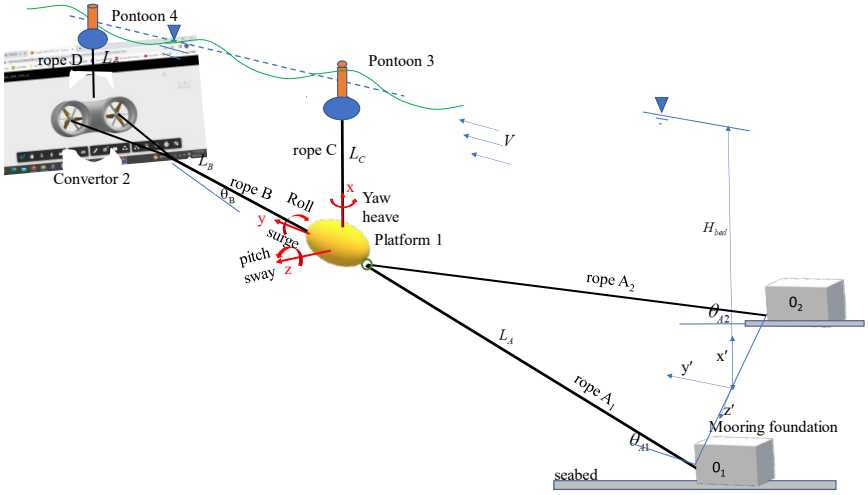

Figure 1. Configuration of the mooring system for the ocean energy convertor.

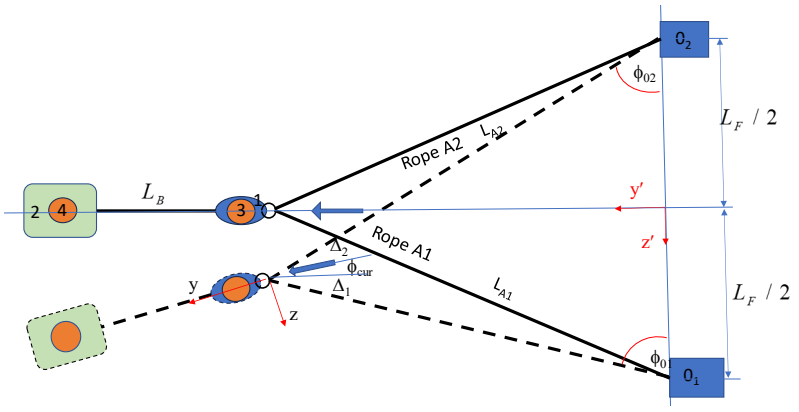

Figure 2. Top view of the mooring system of ocean energy convertor.

The global translational and the rotational displacements of the components are.

$$x_i = x_{is} + x_{id}, \quad y_i = y_{is} + y_{id}, \quad z_i = z_{is} + z_{id}, \quad i = 1,\ 2,\ 3,\ 4$$

$$\varphi_{jx} = \varphi_{jxs} + \varphi_{jxd},\ \varphi_{jx} = \varphi_{jxs} + \varphi_{jxd},\ \varphi_{jx} = \varphi_{jxs} + \varphi_{jxd};\ \varphi_{jxs} = \varphi_{jxs} = \varphi_{jxs} = 0, j = 1,2 \quad (1)$$

The total tensions of the ropes are

 doi:10.20944/preprints202407.1940.v1

$$T_i = T_{is} + T_{id}, \quad i = A,\ B,\ C,\ D \tag{2}$$

These displacements and tensions include (1) the static one under the steady current only, (2) the dynamic one due to the wave impact and current. Because rope A connects to the pulley fixed to the platform and two foundations, the tension of rope A_1 is equal to that of rope A_2, $T_{A1} = T_{A2} = T_A$, $T_{A1s} = T_{A2s} \equiv T_{As}$ and $T_{A1d} = T_{A2d} \equiv T_{Ad}$.

3. Static Displacements and Equilibrium under the Steady Current only

3.1. Static Displacements

Under the steady current only, the static displacements of the components are

Foundation:

$$x'_{01} = 0, \qquad y'_{01} = 0, \qquad z'_{01} = L_F / 2, \tag{3}$$

$$x'_{02} = 0, \qquad y'_{02} = 0, \qquad z'_{02} = -L_F / 2, \tag{4}$$

Platform:

$$x'_{1s} = H_{bed} - L_C = L_{A1} \sin\theta_{As1} = L_{A2} \sin\theta_{As2}, \tag{5}$$

$$y'_{1s} = L_{A1} \cos\theta_{As1} \sin\phi_{01} = L_{A2} \cos\theta_{As2} \sin\phi_{02} \tag{6}$$

$$z'_{1s} = L_F / 2 - L_{A1} \cos\theta_{As1} \cos\phi_{01} = -L_F / 2 + L_{A2} \cos\theta_{As2} \cos\phi_{02} \tag{7}$$

The lengths of rope A_1 and A_2 are

$$L_{A1} = \sqrt{\left(x'_{1s} - x'_{01}\right)^2 + \left(y'_{1s} - y'_{01}\right)^2 + \left(z'_{1s} - z'_{01}\right)^2} \tag{8}$$

$$L_{A2} = \sqrt{\left(x'_{1s} - x'_{02}\right)^2 + \left(y'_{1s} - y'_{02}\right)^2 + \left(z'_{1s} - z'_{02}\right)^2} \tag{9}$$

$$L_A = L_{A1} + L_{A2} \tag{10}$$

The static displacements and parameters of mooring system, $\{y_{1s}, z_{1s}\}$ and $\{L_{A1}, L_{A2}, \theta_{As1}, \theta_{As2}, \phi_{01}, \phi_{02}\}$ change with the current direction ϕ_{cur}. These parameters can be determined by using the static equilibrium principle later.

Turbine:

$$x'_{2s} = H_{bed} - L_D = x'_{1s} - L_B \sin\theta_{Bs}, \tag{11}$$

$$y'_{2s} = y'_{1s} + L_B \cos\theta_{Bs} \cos\phi_{cur}, \tag{12}$$

$$z'_{2s} = z'_{1s} + L_B \cos\theta_{Bs} \sin\phi_{cur}, \tag{13}$$

Pontoons 3, 4:

$$x'_{3s} = x'_{1s} + L_C = H_{bed}, \qquad y'_{3s} = y'_{1s}, \qquad z'_{3s} = z'_{1s}, \tag{14}$$

$$x'_{4s} = x'_{3s} = x'_{2s} + L_D = H_{bed}, \qquad y'_{4s} = y'_{2s}, \qquad z'_{4s} = z'_{2s}, \tag{15}$$

Rotational angles of platform and convertor:

$$\varphi_{jks} = 0,\ j = 1,2;\ k = x, y, z \tag{16}$$

The global setting angle qBs of rope B is

$$\sin\theta_{Bs} = \left(x_{1s} - x_{2s}\right) / L_B \tag{17}$$

The relation between the x-y-z and x′-y′-z′ coordinates is

$$\vec{r}_p = x_p \vec{i} + y_p \vec{j} + z_p \vec{k};\ p = 01, 02, 1s, 2s, 3s, 4s \tag{18}$$

where

$$x_p = \left(x'_p - x'_{1s}\right), \quad y_p = \left[\left(y'_p - y'_{1s}\right)\cos\phi_{cur} + \left(z'_p - z'_{1s}\right)\sin\phi_{cur}\right],$$
$$z_p = \left[-\left(y'_p - y'_{1s}\right)\sin\phi_{cur} + \left(z'_p - z'_{1s}\right)\cos\phi_{cur}\right] \tag{19}$$

3.2. Static Force Equilibrium

 doi:10.20944/preprints202407.1940.v1

Under the steady current only, the static equilibrium of the energy convertor in the current direction is

$$T_{\mathrm{Bs}}\cos\theta_{Bs}=f_{Tys} \tag{20}$$

where the drag of the convertor under steady current $f_{Tys}=0.5C_{DTy}\rho A_{TY}V^2$. The static equilibrium of the platform in the current direction is

$$T_{\mathrm{As}1}\cos\theta_{As1}\cos\left(\Delta_1+\phi_{cur}\right)+T_{\mathrm{As}2}\cos\theta_{As2}\cos\Delta_2=f_{Pys}+f_{Tys} \tag{21}$$

where the drag of the platform under steady current $f_{Pys}=0.5C_{DPy}\rho A_{PY}V^2$, $\Delta_1=\left(\pi/2-\phi_{01}\right)$ and $\Delta_2=\left(\pi/2-\phi_{02}\right)-\phi_{cur}$. Because the rope A connects to the pulley, as shown in Figure 2, the tensions of ropes A_1 and A_2 are

$$T_{\mathrm{As}1}=T_{\mathrm{As}2}=T_{\mathrm{As}} \tag{22}$$

Based on Equations (20-22), the static tension of rope A is expressed as

$$T_{\mathrm{As}}=\frac{f_{Pys}+f_{Tys}}{\cos\theta_{As1}\cos\left(\Delta_1+\phi_{cur}\right)+\cos\theta_{As2}\cos\Delta_2}=\frac{f_{Pys}+T_{\mathrm{Bs}}\cos\theta_{Bs}}{\cos\theta_{As1}\cos\left(\Delta_1+\phi_{cur}\right)+\cos\theta_{As2}\cos\Delta_2} \tag{23}$$

The static equilibrium of the platform in the x-direction is

$$T_{Cs}+F_{B1s}=\left[T_{\mathrm{As}1}\sin\theta_{As1}+T_{\mathrm{As}2}\sin\theta_{As2}\right]+T_{\mathrm{Bs}}\sin\theta_{Bs}+W_1 \tag{24}$$

The static equilibrium of the platform in the z-direction is

$$\cos\theta_{As1}\sin\left(\Delta_1+\phi_{cur}\right)-\cos\theta_{As2}\sin\Delta_2=0 \tag{25}$$

The static equilibrium of the energy convertor in the x-direction is

$$T_{\mathrm{Ds}}=W_2-T_{\mathrm{Bs}}\sin\theta_{Bs}-F_{B2s} \tag{26}$$

The static equilibrium of the pontoon 3 in the x-direction is

$$F_{B3s}=W_3+T_{Cs} \tag{27}$$

The static equilibrium of the pontoon 4 in the x-direction is

$$F_{B4s}=W_4+T_{\mathrm{Ds}} \tag{28}$$

3.3. Solution Method of Static Equilibrium and Displacements

Substituting Equations (7-9) into Equation (25), one obtains

$$\begin{aligned}&\cos\theta_{As1}\left[\sin\left(\pi/2+\phi_{cur}\right)\cos\phi_{01}-\cos\left(\pi/2+\phi_{cur}\right)\sin\phi_{01}\right]\\&-\cos\theta_{As2}\left[\sin\left(\pi/2-\phi_{cur}\right)\cos\phi_{02}-\cos\left(\pi/2-\phi_{cur}\right)\sin\phi_{02}\right]=0\end{aligned} \tag{29}$$

where $\theta_{As1}=\sin^{-1}\dfrac{H_{bed}-L_C}{L_{A1}}$, $\theta_{As2}=\sin^{-1}\dfrac{H_{bed}-L_C}{L_A-L_{A1}}$,

$\phi_{02}=\cos^{-1}\left(\dfrac{a_2^2+L_F^2-a_1^2}{2L_Fa_2}\right)$, $\phi_{01}=\cos^{-1}\left(\dfrac{L_F-a_2\cos\phi_{02}}{a_1}\right)$,

$a_1=L_{A1}\cos\theta_{As1}$, $a_2=L_{A2}\cos\theta_{As2}$.

If the basic parameters $\{\phi_{cur},H_{bed},L_C,L_A,L_F\}$ are given, the length of rope A_1, L_{A1}, can be determined by using the bisection method via Equation (29). Substituting L_{A1} back into Equations (8-9,12-17), the parameters $\{L_{A2},\theta_{As1},\theta_{As2},\ \phi_{01},\phi_{02},y'_{1s},z'_{1s}\}$ are obtained.

3.4. Static Numerical Results

Parameters of the mooring system are listed in Table 1.

Table 1. the parameters of the system.

parameter	dimension	parameter	dimension
depth of seabed H_{bed}	1300m	current velocity V	1.5m/s

 doi:10.20944/preprints202407.1940.v1

length of rope *A*, L_A	5200m	length of rope *B*, L_B	170m
length of rope *C*, L_C	60m	length of rope *D*, L_D	140m
Static drag of the invertor F_{DT}	59.35 tons	Static drag of the platform F_{DB}	0.077 tons

Figure 3 demonstrates that the convertor direction is almost same as current. The distance L_F between two foundations increases slightly the deviation of the convertor direction from current.

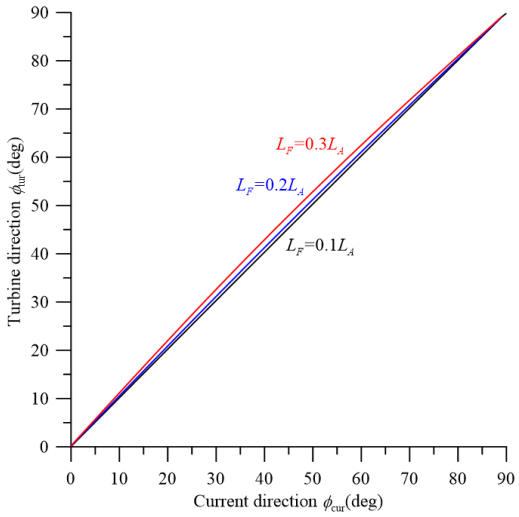

Figure 3. relation between the directions of invertor and current.

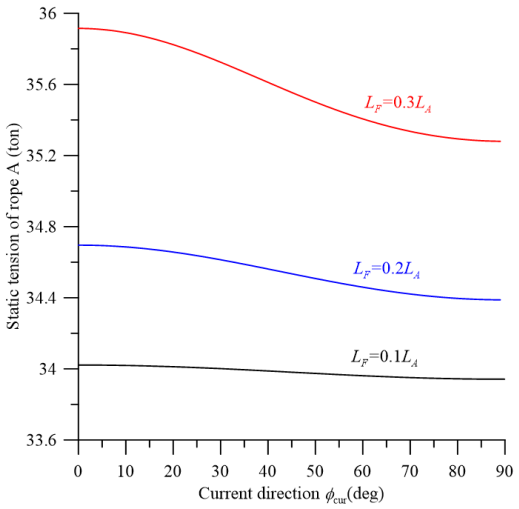

Figure 4. effect of current direction on tension of rope *A*.

Figure 4 shows the effects of the current direction and the distance L_F between two foundations on the static tension of rope *A*, T_{As}. If the current velocity V_{cur}=1.5m/s, the drag of the convertor F_{DT}=59.35tons and the drag of the platform F_{DB}=0.077tons. If the traditional single traction rope is considered, the corresponding rope length is 2480m and the tension T_{As} =68.62tons. However, if L_F =0.1L_A in this proposed system, the tension T_{As} is about 34tons only. It is half of the traditional traction rope. The current direction φ_{cur} decreases the static tension T_{As}. Moreover, the larger the distance L_F is, the larger the static tension T_{As} is.

4. Dynamic Analysis

 doi:10.20944/preprints202407.1940.v1

4.1. Similarity of System

4.1.1. Hydrodynamic Similarity of Convertor

Lin *et al.* [8] presented the hydrodynamic coefficients of fluid-structure interaction of a 400kW turbine and platform determined by using computational fluid dynamics method. An ocean current convertor of MW level is commercial specification. In this study, the dynamic response of a 1 MW turbine mooring system will be investigated. The corresponding hydrodynamic coefficients and other parameters are determined based on the similarity law and the presented parameters [8]. The similarity law is presented as follows:

Similarity of tip speed ratio (TSR):

$$\left(\frac{\omega_T D_T}{V_{cur}}\right)_{\text{mod}} = \left(\frac{\omega_T D_T}{V_{cur}}\right)_{pro} \tag{30}$$

Lin *et al*. [8] proposed that *TSR*=3.5 for the 400kW turbine, the efficiency is maximum. Considering the same current velocity V_{cur} for the model and prototype, Equation (31) becomes

$$\frac{\omega_{T,mod}}{\omega_{T,pro}} = \frac{D_{T,pro}}{D_{T,mod}} \tag{31}$$

Similarity of power number N_P:

$$\left(\frac{Power}{\rho D_T^5 \omega_T^3}\right)_{\text{model}} = \left(\frac{Power}{\rho D_T^5 \omega_T^3}\right)_{prototype} \tag{32}$$

Considering the same current velocity V_{cur} and sea density r for the model and prototype and substituting Equation (31) into Equation (32),

$$\frac{D_{T,pro}}{D_{T,\text{mod}}} = \sqrt{\frac{Power_{pro}}{Power_{\text{mod}}}}. \tag{33}$$

Similarity of hydrodynamic force and moment for convertor:

The hydrodynamic force of convertor is

$$\begin{aligned} f_{Tj}\left(V_{cur},\dot{x}_T,\dot{y}_T,\dot{z}_T,\varphi_{Tx},\varphi_{Ty},\varphi_{Tz},\dot{\varphi}_{Tx},\dot{\varphi}_{Ty},\dot{\varphi}_{Tz},TSR\right) &\equiv f_{Tj}\left(V_{cur},s_{T1},s_{T2},s_{T3},s_{T4},s_{T5},s_{T6},s_{T7},s_{T8},s_{T9},TSR\right) \\ = f_{Tj,0}\left(V_{cur},0,0,0,0,0,0,0,0,0,TSR\right) &+ \sum_{k=1}^{9} s_{Tk}\left.\frac{\partial f_{Tj}}{\partial s_{Tk}}\right|_{s_{Ti}=0,i\neq k}, j=x,y,z \end{aligned} \tag{34}$$

Dividing Equation(34) by $\frac{1}{2}\rho A_{tur} V_{cur}^2$, it becomes one in terms of dimensionless variables

$$\begin{aligned} C_{fTj}\left(V_{cur},\dot{x}_T,\dot{y}_T,\dot{z}_T,\varphi_{Tx},\varphi_{Ty},\varphi_{Tz},\dot{\varphi}_{Tx},\dot{\varphi}_{Ty},\dot{\varphi}_{Tz},TSR\right) &\equiv C_{fTj}\left(V_{cur},s_{T1},s_{T2},s_{T3},s_{T4},s_{T5},s_{T6},s_{T7},s_{T8},s_{T9},TSR\right) \\ = C_{fTj,0}\left(V_{cur},0,0,0,0,0,0,0,0,0,TSR\right) &+ \sum_{k=1}^{9} \tilde{s}_{Tk}\left.\frac{\partial C_{fTj}}{\partial \tilde{s}_{Tk}}\right|_{s_i=0,i\neq k}, j=x,y,z \end{aligned} \tag{35}$$

where

$$C_{fTj} = \frac{f_{Tj}}{\frac{1}{2}\rho A_{tur} V_{cur}^2},\quad \tilde{s}_{Tk} = \frac{s_{Tk}}{\xi_T},\quad \xi_T = \begin{cases} V_{cur}, & s_{Tk} = \dot{x}_T,\dot{y}_T,\dot{z}_T \\ 1, & s_{Tk} = \varphi_{Tx},\varphi_{Ty},\varphi_{Tz} \\ \omega_T, & s_{Tk} = \dot{\varphi}_{Tx},\dot{\varphi}_{Ty},\dot{\varphi}_{Tz} \end{cases}. \tag{36}$$

If the prototype and the model are similar, their dimensionless force coefficients (35) are same

$$\left[C_{fTj}\right]_{pro} = \left[C_{fTj}\right]_{\text{mod}} \tag{37}$$

Based on Equations (35-37), one can obtain the following similar parameters

Similarity of drag force coefficient is

$$\left[C_{fTj,0}\left(V_{cur},0,0,0,0,0,0,0,0,0,TSR\right)\right]_{\text{mod}} = \left[C_{fTj,0}\left(V_{cur},0,0,0,0,0,0,0,0,0,TSR\right)\right]_{pro}, j=x,y,z \tag{38}$$

Similarity of hydrodynamic damping force coefficient:

 doi:10.20944/preprints202407.1940.v1

$$\left(\frac{\partial C_{fTj}}{\partial \tilde{s}_{Tk}}\bigg|_{s_{Ti}=0,i\neq k}\right)_{\text{mod}}=\left(\frac{\partial C_{fTj}}{\partial \tilde{s}_{Tk}}\bigg|_{s_{Ti}=0,i\neq k}\right)_{pro},\ j=x,y,z \quad ;\ s_{Tk}=\dot{x}_T,\dot{y}_T,\dot{z}_T,\dot{\varphi}_{Tx},\dot{\varphi}_{Ty},\dot{\varphi}_{Tz} \tag{39}$$

Similarity of hydrodynamic stiffness force coefficient:

$$\left(\frac{\partial C_{fTj}}{\partial \varphi_{Tk}}\bigg|_{\varphi_{Ti}=0,i\neq k}\right)_{\text{mod}}=\left(\frac{\partial C_{fTj}}{\partial \varphi_{Tk}}\bigg|_{\varphi_{Ti}=0,i\neq k}\right)_{pro},\ j=x,y,z \quad ;\ s_{Tk}=\varphi_{Tx},\varphi_{Ty},\varphi_{Tz} \tag{40}$$

Based on the similar formula (36, 39, 40), the hydrodynamic damping force relations between the model and prototype

$$\left(\frac{\partial f_{Tj}}{\partial s_{Tk}}\bigg|_{s_{Ti}=0,i\neq k}\right)_{\text{pro}}=\frac{D_{T,pro}^2}{D_{T,\text{mod}}^2}\left(\frac{\partial f_{Tj}}{\partial s_{Tk}}\bigg|_{s_{Ti}=0,i\neq k}\right)_{\text{mod}},\ j=x,y,z;\ s_{Tk}=\dot{x}_T,\dot{y}_T,\dot{z}_T \tag{41}$$

$$\left(\frac{\partial f_{Tj}}{\partial \dot{\varphi}_{Tk}}\bigg|_{\dot{\varphi}_{Tk}=0,i\neq k}\right)_{pro}=\frac{D_{T,pro}^2}{D_{T,mod}^2}\frac{\omega_{mod}}{\omega_{pro}}\left(\frac{\partial f_{Tj}}{\partial \dot{\varphi}_{Tk}}\bigg|_{\varphi_{Tk}=0,i\neq k}\right)_{mod},\ j,k=x,y,z \tag{42}$$

and the hydrodynamic stiffness force relation

$$\left(\frac{\partial f_{Tj}}{\partial \varphi_{Tk}}\bigg|_{\varphi_{Tk}=0,i\neq k}\right)_{\text{pro}}=\frac{D_{T,pro}^2}{D_{T,\text{mod}}^2}\left(\frac{\partial f_{Tj}}{\partial \varphi_{Tk}}\bigg|_{\varphi_{Tk}=0,i\neq k}\right)_{\text{mod}},\ j,k=x,y,z \tag{43}$$

Given the coefficients of the model and substituting Equations (31, 33) into Equations (41-43), the hydrodynamic damping and stiffness force coefficients of the prototype can be obtained.

According to the similarity of drag force coefficient (38), the drag force relation is

$$\frac{\left(f_{Ty,0}\right)_{pro}}{\left(f_{Ty,0}\right)_{\text{mod}}}=\frac{D_{T,pro}^2}{D_{T,\text{mod}}^2} \tag{44}$$

Based on Equation (44), the similarity of fracture strength of rope is

$$\frac{T_{frac,pro}}{T_{frac,\text{mod}}}=\frac{\left(f_{Ty,0}\right)_{pro}}{\left(f_{Ty,0}\right)_{\text{mod}}}=\frac{D_{T,pro}^2}{D_{T,\text{mod}}^2} \tag{45}$$

The hydrodynamic moment of convertor is

$$\begin{aligned} m_{Tj}\left(V_{cur},\dot{x}_T,\dot{y}_T,\dot{z}_T,\varphi_{Tx},\varphi_{Ty},\varphi_{Tz},\dot{\varphi}_{Tx},\dot{\varphi}_{Ty},\dot{\varphi}_{Tz},TSR\right)&\equiv m_{Tj}\left(V_{cur},s_{T1},s_{T2},s_{T3},s_{T4},s_{T5},s_{T6},s_{T7},s_{T8},s_{T9},TSR\right)\\ &=m_{Tj,0}\left(V_{cur},0,0,0,0,0,0,0,0,0,TSR\right)+\sum_{k=1}^{9}s_{Tk}\frac{\partial m_{Tj}}{\partial s_{Tk}}\bigg|_{s_{Ti}=0,i\neq k},\ j=x,y,z \end{aligned} \tag{46}$$

Dividing Equation (46) by $\frac{1}{2}\rho D_T A_{tur} V_{cur}^2$, it becomes one in terms of dimensionless variables

$$\begin{aligned} C_{mTj}\left(V_{cur},\dot{x}_T,\dot{y}_T,\dot{z}_T,\varphi_{Tx},\varphi_{Ty},\varphi_{Tz},\dot{\varphi}_{Tx},\dot{\varphi}_{Ty},\dot{\varphi}_{Tz},TSR\right)&\equiv C_{mTj}\left(V_{cur},s_{T1},s_{T2},s_{T3},s_{T4},s_{T5},s_{T6},s_{T7},s_{T8},s_{T9},TSR\right)\\ &=C_{mTj,0}\left(V_{cur},0,0,0,0,0,0,0,0,0,TSR\right)+\sum_{k=1}^{9}\tilde{s}_{Tk}\frac{\partial C_{mTj}}{\partial \tilde{s}_{Tk}}\bigg|_{s_{Ti}=0,i\neq k},\ j=x,y,z \end{aligned} \tag{47}$$

where $C_{mTj}=m_{Tj}/\left(\frac{1}{2}\rho D_T A_{tur} V_{cur}^2\right)$.

If the prototype and the model are similar, the two dimensionless moments (47) are same

$$\left[C_{mTj}\right]_{pro}=\left[C_{mTj}\right]_{\text{mod}} \tag{48}$$

Based on Equations (47-48), one can obtain the following similar parameters

Similarity of drag moment coefficient is

$$\left[C_{mTj,0}\left(V_{cur},0,0,0,0,0,0,0,0,0,TSR\right)\right]_{\text{mod}}=\left[C_{mTj,0}\left(V_{cur},0,0,0,0,0,0,0,0,0,TSR\right)\right]_{pro},\ j=x,y,z \tag{49}$$

Similarity of hydrodynamic damping in moment:

 doi:10.20944/preprints202407.1940.v1

$$\left(\frac{\partial C_{mTj}}{\partial \tilde{s}_{Tk}}\bigg|_{s_{Ti}=0,i\neq k}\right)_{\text{mod}}=\left(\frac{\partial C_{mTj}}{\partial \tilde{s}_{Tk}}\bigg|_{s_{Ti}=0,i\neq k}\right)_{pro},\ j=x,y,z \quad ;\ s_k=\dot{x}_T,\dot{y}_T,\dot{z}_T,\dot{\varphi}_{Tx},\dot{\varphi}_{Ty},\dot{\varphi}_{Tz} \tag{50}$$

Similarity of hydrodynamic stiffness in moment:

$$\left(\frac{\partial C_{mTj}}{\partial \varphi_{Tk}}\bigg|_{\varphi_{Ti}=0,i\neq k}\right)_{\text{mod}}=\left(\frac{\partial C_{mTj}}{\partial \varphi_{Tk}}\bigg|_{\varphi_{Ti}=0,i\neq k}\right)_{pro},\ j=x,y,z \quad ;\ s_k=\varphi_{Tx},\varphi_{Ty},\varphi_{Tz} \tag{51}$$

Based on the similar formula (36, 50-51), the hydrodynamic damping moment relations between the model and prototype

$$\left(\frac{\partial m_{Tj}}{\partial s_{Tk}}\bigg|_{s_{Tk}=0,i\neq k}\right)_{pro}=\frac{D_{T,pro}^3}{D_{T,\text{mod}}^3}\left(\frac{\partial m_{Tj}}{\partial s_{Tk}}\bigg|_{s_{Tk}=0,i\neq k}\right)_{\text{mod}},\ s_{Tk}=\dot{x}_T,\dot{y}_T,\dot{z}_T \tag{52}$$

$$\left(\frac{\partial m_{Tj}}{\partial \dot{\varphi}_{Tk}}\bigg|_{\dot{\varphi}_{Tk}=0,i\neq k}\right)_{pro}=\frac{D_{T,pro}^3}{D_{T,\text{mod}}^3}\frac{\omega_{T,\text{mod}}}{\omega_{T,pro}}\left(\frac{\partial m_{Tj}}{\partial \dot{\varphi}_{Tk}}\bigg|_{\dot{\varphi}_{Tk}=0,i\neq k}\right)_{\text{mod}},\quad j,k=x,y,z \tag{53}$$

and the hydrodynamic stiffness moment relation

$$\left(\frac{\partial m_{Tj}}{\partial \varphi_{Tk}}\bigg|_{\varphi_{Tk}=0,i\neq k}\right)_{pro}=\frac{D_{T,pro}^3}{D_{T,\text{mod}}^3}\left(\frac{\partial m_{Tj}}{\partial \varphi_{Tk}}\bigg|_{\varphi_{Tk}=0,i\neq k}\right)_{\text{mod}},\quad j,k=x,y,z \tag{54}$$

Given the coefficients of the model and substituting Equations (31, 33) into Equations (52-54), the hydrodynamic damping and stiffness moment coefficients of the prototype can be obtained.

4.1.2. Hydrodynamic Similarity of Platform

The hydrodynamic force of platform is

$$\begin{aligned} &f_{Pj}\left(V_{cur},\dot{x}_P,\dot{y}_P,\dot{z}_P,\varphi_{Px},\varphi_{Py},\varphi_{Pz},\dot{\varphi}_{Px},\dot{\varphi}_{Py},\dot{\varphi}_{Pz}\right)\equiv f_{Pj}\left(V_{cur},s_{P1},s_{P2},s_{P3},s_{P4},s_{P5},s_{P6},s_{P7},s_{P8},s_{P9}\right)\\ &=f_{Pj,0}\left(V_{cur},0,0,0,0,0,0,0,0,0\right)+\sum_{k=1}^{9}s_{Pk}\frac{\partial f_{Pj}}{\partial s_{Pk}}\bigg|_{s_i=0,i\neq k},\ j=x,y,z \end{aligned} \tag{55}$$

Dividing Equation(55) by $\frac{1}{2}\rho A_{pla}V_{cur}^2$, it becomes in terms of dimensionless variables

$$\begin{aligned} &C_{fPj}\left(V_{cur},\dot{x}_P,\dot{y}_P,\dot{z}_P,\varphi_{Px},\varphi_{Py},\varphi_{Pz},\dot{\varphi}_{Px},\dot{\varphi}_{Py},\dot{\varphi}_{Pz}\right)\equiv C_{fPj}\left(V_{cur},s_{P1},s_{P2},s_{P3},s_{P4},s_{P5},s_{P6},s_{P7},s_{P8},s_{P9}\right)\\ &=C_{fPj,0}\left(V_{cur},0,0,0,0,0,0,0,0,0\right)+\sum_{k=1}^{9}\tilde{s}_{Pk}\frac{\partial C_{fPj}}{\partial \tilde{s}_{Pk}}\bigg|_{s_{Pi}=0,i\neq k},\ j=x,y,z \end{aligned} \tag{56}$$

where

$$C_{fPj}=\frac{f_{Pj}}{\frac{1}{2}\rho A_{pla}V_{cur}^2},\quad \tilde{s}_{Pk}=\frac{s_{Pk}}{\xi_P},\quad \xi_P=\begin{cases}V_{cur}, & s_{Pk}=\dot{x}_P,\dot{y}_P,\dot{z}_P\\ 1, & s_{Pk}=\varphi_{Px},\varphi_{Py},\varphi_{Pz}\\ \omega_T, & s_{Pk}=\dot{\varphi}_{Px},\dot{\varphi}_{Py},\dot{\varphi}_{Pz}\end{cases}. \tag{57}$$

If the prototype and the model are similar, the two dimensionless force coefficients (56) are same

$$\left[C_{fPj}\right]_{pro}=\left[C_{fPj}\right]_{\text{mod}} \tag{58}$$

Based on Equations (56-58), one can obtain the following similar parameters.

Similarity of hydrodynamic damping force coefficient:

$$\left(\frac{\partial C_{fPj}}{\partial \tilde{s}_{Pk}}\bigg|_{s_{Pi}=0,i\neq k}\right)_{\text{mod}}=\left(\frac{\partial C_{fPj}}{\partial \tilde{s}_{Pk}}\bigg|_{s_{Pi}=0,i\neq k}\right)_{pro},\ j=x,y,z \quad ;\ s_{Pk}=\dot{x}_P,\dot{y}_P,\dot{z}_P,\dot{\varphi}_{Px},\dot{\varphi}_{Py},\dot{\varphi}_{Pz} \tag{59}$$

Similarity of hydrodynamic stiffness force coefficient:

$$\left(\frac{\partial C_{fPj}}{\partial \varphi_{Pk}}\bigg|_{\varphi_{Pi}=0,i\neq k}\right)_{\text{mod}}=\left(\frac{\partial C_{fPj}}{\partial \varphi_{Pk}}\bigg|_{\varphi_{Pi}=0,i\neq k}\right)_{pro},\ j=x,y,z \quad ;\ s_{Pk}=\varphi_{Px},\varphi_{Py},\varphi_{Pz} \tag{60}$$

 doi:10.20944/preprints202407.1940.v1

Based on Equations (57, 59-60), the hydrodynamic damping force relations between the model and prototype

$$\left(\left.\frac{\partial f_{Pj}}{\partial s_{Pk}}\right|_{s_{Pi}=0,i\neq k}\right)_{\text{pro}}=\frac{D_{P,\,pro}^2}{D_{P,\text{mod}}^2}\left(\left.\frac{\partial f_{Pj}}{\partial s_{Pk}}\right|_{s_{Ti}=0,i\neq k}\right)_{\text{mod}},\ j=x,y,z;\ s_{Pk}=\dot{x}_P,\dot{y}_P,\dot{z}_P \tag{61}$$

$$\left(\left.\frac{\partial f_{Pj}}{\partial \dot{\varphi}_{Pk}}\right|_{\dot{\varphi}_{Pk}=0,i\neq k}\right)_{pro}=\frac{D_{P,\,pro}^2}{D_{P,mod}^2}\frac{\omega_{T,mod}}{\omega_{T,pro}}\left(\left.\frac{\partial f_{Pj}}{\partial \dot{\varphi}_{Pk}}\right|_{\dot{\varphi}_{Pk}=0,i\neq k}\right)_{mod},\ j,k=x,y,z \tag{62}$$

and the hydrodynamic stiffness force relation

$$\left(\left.\frac{\partial f_{Pj}}{\partial \varphi_{Pk}}\right|_{\varphi_{Tk}=0,i\neq k}\right)_{\text{pro}}=\frac{D_{P,\,pro}^2}{D_{P,\text{mod}}^2}\left(\left.\frac{\partial f_{Pj}}{\partial \varphi_{Pk}}\right|_{\varphi_{Pk}=0,i\neq k}\right)_{\text{mod}},\ j,k=x,y,z \tag{63}$$

Given the coefficients of the model and substituting Equations (31, 33) into Equations (61-63), the hydrodynamic damping and stiffness force coefficients of the prototype can be obtained.

The hydrodynamic moment of platform is

$$\begin{aligned}&m_{Pj}\left(V_{cur},\dot{x}_P,\dot{y}_P,\dot{z}_P,\varphi_{Px},\varphi_{Py},\varphi_{Pz},\dot{\varphi}_{Px},\dot{\varphi}_{Py},\dot{\varphi}_{Pz}\right)\equiv m_{Pj}\left(V_{cur},s_{P1},s_{P2},s_{P3},s_{P4},s_{P5},s_{P6},s_{P7},s_{P8},s_{P9}\right)\\&=m_{Pj,0}\left(V_{cur},0,0,0,0,0,0,0,0,0\right)+\sum_{k=1}^{9}s_{Pk}\left.\frac{\partial m_{Pj}}{\partial s_{Pk}}\right|_{s_{Pi}=0,i\neq k},\ j=x,y,z\end{aligned} \tag{64}$$

Dividing Equation(64) by $\frac{1}{2}\rho D_P A_{pla} V_{cur}^2$, it becomes one in terms of dimensionless variables

$$\begin{aligned}&C_{mPj}\left(V_{cur},\dot{x}_P,\dot{y}_P,\dot{z}_P,\varphi_{Px},\varphi_{Py},\varphi_{Pz},\dot{\varphi}_{Px},\dot{\varphi}_{Py},\dot{\varphi}_{Pz}\right)\equiv C_{mTj}\left(V_{cur},s_{P1},s_{P2},s_{P3},s_{P4},s_{P5},s_{P6},s_{P7},s_{P8},s_{P9}\right)\\&=C_{mPj,0}\left(V_{cur},0,0,0,0,0,0,0,0,0\right)+\sum_{k=1}^{9}\tilde{s}_{Pk}\left.\frac{\partial C_{mPj}}{\partial \tilde{s}_{Pk}}\right|_{s_{Pi}=0,i\neq k},\ j=x,y,z\end{aligned} \tag{65}$$

where $C_{mPj}=m_{Pj}/\left(\frac{1}{2}\rho D_P A_{pla} V_{cur}^2\right)$.

If the prototype and the model are similar, their dimensionless moments (65) are same

$$\left[C_{mPj}\right]_{pro}=\left[C_{mPj}\right]_{\text{mod}} \tag{66}$$

Based on Equations (63-64), one can obtain the following similar parameters.

Similarity of drag moment coefficient is

$$\left[C_{mPj,0}\left(V_{cur},0,0,0,0,0,0,0,0,0\right)\right]_{\text{mod}}=\left[C_{mPj,0}\left(V_{cur},0,0,0,0,0,0,0,0,0\right)\right]_{pro},\ j=x,y,z \tag{67}$$

Similarity of hydrodynamic damping in moment:

$$\left(\left.\frac{\partial C_{mPj}}{\partial \tilde{s}_{Pk}}\right|_{s_{Pi}=0,i\neq k}\right)_{\text{mod}}=\left(\left.\frac{\partial C_{mPj}}{\partial \tilde{s}_{Pk}}\right|_{s_{Pi}=0,i\neq k}\right)_{pro},\ j=x,y,z\ ;\ s_{Pk}=\dot{x}_P,\dot{y}_P,\dot{z}_P,\dot{\varphi}_{Px},\dot{\varphi}_{Py},\dot{\varphi}_{Pz} \tag{68}$$

Similarity of hydrodynamic stiffness in moment:

$$\left(\left.\frac{\partial C_{mPj}}{\partial \varphi_{Pk}}\right|_{s_{Pi}=0,i\neq k}\right)_{\text{mod}}=\left(\left.\frac{\partial C_{mPj}}{\partial \varphi_{Pk}}\right|_{s_{Pi}=0,i\neq k}\right)_{pro},\ j,k=x,y,z\ ; \tag{69}$$

Based on the similar formula (36, 68-69), the hydrodynamic damping moment relations between the model and prototype

$$\left(\left.\frac{\partial m_{Pj}}{\partial s_{Pk}}\right|_{s_{Pk}=0,i\neq k}\right)_{pro}=\frac{D_{P,\,pro}^3}{D_{P,\text{mod}}^3}\left(\left.\frac{\partial m_{Pj}}{\partial s_{Pk}}\right|_{s_{Pk}=0,i\neq k}\right)_{\text{mod}},\ s_{Pk}=\dot{x}_P,\dot{y}_P,\dot{z}_P \tag{70}$$

$$\left(\left.\frac{\partial m_{Pj}}{\partial \dot{\varphi}_{Pk}}\right|_{\dot{\varphi}_{Pk}=0,i\neq k}\right)_{pro}=\frac{D_{P,\,pro}^3}{D_{P,\text{mod}}^3}\frac{\omega_{T,\text{mod}}}{\omega_{T,pro}}\left(\left.\frac{\partial m_{Pj}}{\partial \dot{\varphi}_{Pk}}\right|_{\dot{\varphi}_{Pk}=0,i\neq k}\right)_{\text{mod}},\ j,k=x,y,z \tag{71}$$

and the hydrodynamic stiffness moment relation

 doi:10.20944/preprints202407.1940.v1

$$\left(\frac{\partial m_{Pj}}{\partial \varphi_{Pk}}\bigg|_{\varphi_{Pk}=0,i\neq k}\right)_{pro}=\frac{D_{P,pro}^3}{D_{P,\mathrm{mod}}^3}\left(\frac{\partial m_{Pj}}{\partial \varphi_{Pk}}\bigg|_{\varphi_{Pk}=0,i\neq k}\right)_{\mathrm{mod}},\quad j,k=x,y,z \tag{72}$$

Given the coefficients of the model and substituting Equations (31, 33) into Equations (70-72), the hydrodynamic damping and stiffness moment coefficients of the prototype can be obtained.

4.1.3. Geometrical Inertia and Buoyance Similarities

Based on the similarity formula (33) and considering the geometry similarity, one can obtain the similar relations

$$\frac{D_{P,pro}}{D_{P,mod}}=\frac{D_{T,pro}}{D_{T,mod}}=r_d \tag{73}$$

Similarity of mass:

$$\frac{m_{pro}}{m_{\mathrm{mod}}}:\frac{\rho_{pro}Vol_{pro}}{\rho_{\mathrm{mod}}Vol_{\mathrm{mod}}}=r_d^3 \tag{74}$$

Similarity of inertia of mass:

$$\frac{I_{pro}}{I_{\mathrm{mod}}}:\frac{R_{pro}^2 m_{pro}}{R_{\mathrm{mod}}^2 m_{\mathrm{mod}}}=r_d^5 \tag{75}$$

Similarity of buoyance:

$$\frac{F_{Bpro}}{F_{B\mathrm{mod}}}:\frac{\rho_{water}Vol_{pro}}{\rho_{water}Vol_{\mathrm{mod}}}=r_d^3 \tag{76}$$

4.2. Translational Motion in the x-Axis Direction

4.2.1. Equation of Heaving Motion for Pontoon 3

The heaving equation of the pontoon 3 is

$$M_3\ddot{x}_{3d}-K_{Cd}x_{1d}+\left(K_{Cd}+A_{Bx}\rho g\right)x_{3d}=F_{B3d}(t)=\sum_{i=1}^{N}\left[f_{Bs,i}\sin\Omega_i t+f_{Bc,i}\cos\Omega_i t\right] \tag{77}$$

where $F_{B3d}(t)$ is the irregular wave force applied to Pontoon 3, $f_{Bs,i}=A_{Bx}\rho g a_i\cos\varphi_i$ and $f_{Bc,i}=A_{Bx}\rho g a_i\sin\varphi_i$.

The effective spring constant of the rope C- buffer spring connection

$$K_{Cd}=K_{\text{rope C}}/\left(1+K_{\text{rope C}}/K_{C,spring}\right) \tag{78}$$

where $K_{C,spring}$ is the constant of the spring connecting with the rope C. $K_{rope\ C}=E_C A_C/L_C$ in which E_C, A_C, and L_C are the Young's modulus, cross-sectional area and length of the rope C, respectively.

The dynamic tension of the rope C,

$$T_{Cd}=K_{Cd}\delta_{Cd}, \tag{79}$$

where the dynamic elongation between the floating platform 1 and the pontoon 3, $\delta_{Cd}=\left(x_{3d}-x_{1d}\right)$.

4.2.2. Equation of Heaving Motion for Pontoon 4

The heaving equation of the pontoon 4 is

$$M_4\ddot{x}_{4d}-K_{Dd}x_{2d}+\left(K_{Dd}+A_{BT}\rho g\right)x_{4d}=F_{B4d}(t)=\sum_{i=1}^{N}\left[f_{Ts,i}\sin\Omega_i t+f_{Tc,i}\cos\Omega_i t\right] \tag{80}$$

 doi:10.20944/preprints202407.1940.v1

where $F_{B4d}(t)$ is the irregular wave force applied to Pontoon 4. $f_{Ts,i} = A_{BT}\rho g a_i \cos(\varphi_i + \phi_i)$ and $f_{Tc,i} = A_{BT}\rho g a_i \sin(\varphi_i + \phi_i)$. The phase angle $\phi_i = 2\pi L_E \cos\alpha / \lambda_i$ and $L_E = \sqrt{L_B^2 - (L_C - L_D)^2}$. α is the relative wave-current angle, λ_i is the wave length, as shown in Figure 5.

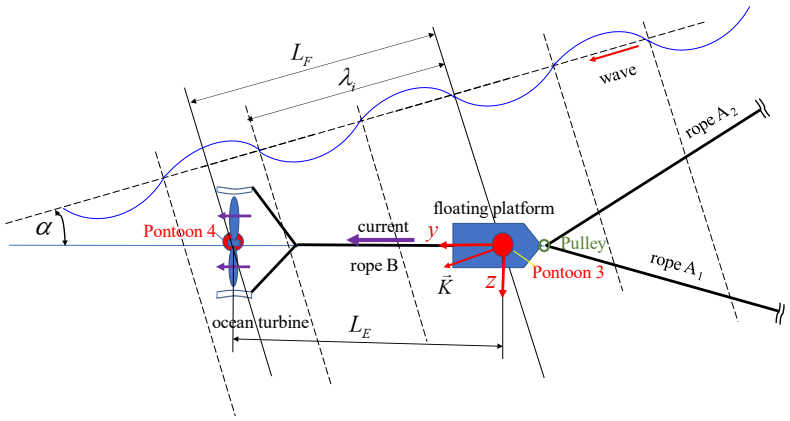

Figure 5. top view of mooring system under wave and current.

The effective spring constant of the rope *D*- buffer spring connection

$$K_{Dd} = K_{\text{rope D}} / \left(1 + K_{\text{rope D}} / K_{D,spring}\right) \tag{81}$$

in which $K_{D,spring}$ is the constant of the spring connecting with the rope *D*. $K_{rope\ D} = E_D A_D / L_D$ where E_D, A_D, and L_D are the Young's modulus, cross-sectional area and length of the rope D, respectively.

The dynamic tension of the rope *C*

$$T_{Dd} = K_{Dd}\delta_{Dd}, \tag{82}$$

where the dynamic elongation between the invertor 2 and the pontoon 4, $\delta_{Dd} = (x_{4d} - x_{2d})$.

4.2.3. Equation of Heaving Motion of the Platform

The dynamic equilibrium of the floating platform in the heaving motion is

$$-(M_1 + m_{eff,x})\ddot{x}_{1d} + f_{\text{Px}} + F_{B1s} - W_1 + T_C - [T_{A1}\sin\theta_{A1} + T_{A2}\sin\theta_{A2}] - T_B \sin\theta_B = 0 \tag{83}$$

where the effective mass $m_{eff,x}$ is derived in Appendix A. The hydrodynamic force on the floating platform due to the fluid-structure interaction (FSI) is expressed in Taylor series as follows:

$$f_{\text{Px}}(V, \dot{x}_{1d}, \dot{y}_{1d}, \dot{z}_{1d}, \varphi_{1x}, \varphi_{1y}, \varphi_{1z}, \dot{\varphi}_{1x}, \dot{\varphi}_{1y}, \dot{\varphi}_{1z}) = f_{Px}(V,0,0,0,0,0,0,0,0,0) + \sum_{j=1}^{9} \frac{\partial f_{Px}}{\partial s_{1j}} s_{1j} + o(s_{1m}s_{1n}) \tag{84}$$

For the briefly, $(\dot{x}_{kd}, \dot{y}_{kd}, \dot{z}_{kd}, \varphi_{kx}, \varphi_{ky}, \varphi_{kz}, \dot{\varphi}_{kx}, \dot{\varphi}_{ky}, \dot{\varphi}_{kz}) \equiv (s_{k1}, s_{k2}, s_{k3}, s_{k4}, s_{k5}, s_{k6}, s_{k7}, s_{k8}, s_{k9})$, $k = 1, 2$. When the symmetry configuration of the platform is considered, the hydrodynamic force on the platform in the x-direction under the current only $f_{Px}(V,0,0,0,0,0,0,0,0,0)$ =0. Considering small oscillation, the higher order terms are neglected later. The right-handed side second term of Equation (84) is the hydrodynamic force due to the fluid-structure interaction.

The dynamic tensions of the ropes *A* and *B* are

$$T_{Ad} = K_{Ad}\delta_{Ad}, \quad T_{Bd} = K_{Bd}\delta_{Bd} \tag{85}$$

The dynamic elongation is the difference between the dynamic and static lengths, $\delta_{\beta d} = L_{\beta d} - L_{\beta s}$, β=*A*, *B*. Using the Taylor formula, the dynamic elongation of rope *A* is derived,

$$\delta_{Ad} = \varepsilon_{AX} x_{1d} + \varepsilon_{AY} y_{1d} + \varepsilon_{AZ} z_{1d} \tag{86}$$

where

$$\varepsilon_{AX} = \frac{(X_A - \varepsilon_{x01})}{r_{A1}} + \frac{(X_A - \varepsilon_{x02})}{r_{A2}}, \quad \varepsilon_{AY} = \frac{(Y_A - \varepsilon_{y01})}{r_{A1}} + \frac{(Y_A - \varepsilon_{y02})}{r_{A2}}$$

 doi:10.20944/preprints202407.1940.v1

$$\varepsilon_{AZ}=\frac{\left(Z_A-\varepsilon_{z01}\right)}{r_{A1}}+\frac{\left(Z_A-\varepsilon_{z02}\right)}{r_{A2}},\quad X_A=\frac{x_{1s}}{L_A},\ Y_A=\frac{y_{1s}}{L_A},\ Z_A=\frac{z_{1s}}{L_A}$$

$$\varepsilon_{x01}=\frac{x_{01}}{L_A},\varepsilon_{y01}=\frac{y_{01}}{L_A},\varepsilon_{z01}=\frac{z_{01}}{L_A},\quad \varepsilon_{x02}=\frac{x_{01}}{L_A},\varepsilon_{y02}=\frac{y_{01}}{L_A},\varepsilon_{z02}=\frac{z_{01}}{L_A},\quad r_{A1}=\frac{L_{A1}}{L_A},\ r_{A2}=\frac{L_{A2}}{L_A}$$

The dynamic elongation of rope *B*

$$\delta_{Bd}=X_B\left(x_{2d}-x_{1d}\right)+Y_B\left(y_{2d}-y_{1d}\right)+Z_B\left(z_{2d}-z_{1d}\right) \tag{87}$$

where $X_B=\frac{\left(x_{2s}-x_{1s}\right)}{L_B},\ Y_B=\frac{\left(y_{2s}-y_{1s}\right)}{L_B},\ Z_B=\frac{\left(z_{2s}-z_{1s}\right)}{L_B}$.

Substituting Equations (84-87) into Equation (83), one obtains

$$\begin{aligned}&-\left(M_1+m_{eff,x}\right)\ddot{x}_{1d}+\left(\sum_{j=1}^{3}\frac{\partial f_{Px}}{\partial s_{1j}}s_{1j}+\sum_{j=7}^{9}\frac{\partial f_{Px}}{\partial s_{1j}}s_{1j}\right)+\sum_{j=4}^{6}\frac{\partial f_{Px}}{\partial s_{1j}}s_{1j}\\&+\left[-K_{Cd}-T_{As}\sum_{i=1}^{2}\left(\frac{\cos\theta_{Ais}}{L_{Ai}}\right)-K_{Ad}\varepsilon_{AX}\sum_{i=1}^{2}\sin\theta_{Ais}+\frac{T_{Bs}\cos\theta_{Bs}}{L_B}+K_{Bd}X_B\sin\theta_{Bs}\right]x_{1d}\\&-\left[\frac{T_{Bs}\cos\theta_{Bs}}{L_B}+K_{Bd}X_B\sin\theta_{Bs}\right]x_{2d}+K_{Cd}x_{3d}+\left(-K_{Ad}\varepsilon_{AY}+K_{Bd}Y_B\sin\theta_{Bs}\right)y_{1d}\\&-K_{Bd}Y_B\sin\theta_{Bs}y_{2d}+\left(-K_{Ad}\varepsilon_{AZ}\sum_{i=1}^{2}\sin\theta_{Ais}+K_{Bd}Z_B\sin\theta_{Bs}\right)z_{1d}-K_{Bd}Z_B\sin\theta_{Bs}z_{2d}=0\end{aligned} \tag{88}$$

4.2.4. Equation of Heaving Motion for the Convertor

The dynamic equilibrium of the convertor in the heaving motion is [8]

$$\begin{aligned}&M_2\ddot{x}_{2d}-\left(\sum_{j=1}^{3}\frac{\partial f_{Tx}}{\partial s_{2j}}s_{1j}+\sum_{j=7}^{9}\frac{\partial f_{Tx}}{\partial s_{2j}}s_{1j}\right)-\sum_{j=4}^{6}\frac{\partial f_{Tx}}{\partial s_{2j}}s_{2j}+\left(\frac{T_{\mathrm{Bs}}\cos\theta_{Bs}}{L_B}+\sin\theta_{Bs}K_{Bd}\frac{\left(x_{2s}-x_{1s}\right)}{L_B}\right)x_{1d}\\&+\left(K_{Dd}-\frac{T_{\mathrm{Bs}}\cos\theta_{Bs}}{L_B}-\sin\theta_{Bs}K_{Bd}\frac{\left(x_{2s}-x_{1s}\right)}{L_B}\right)x_{2d}\\&-K_{Dd}x_{4d}+\sin\theta_{Bs}K_{Bd}\frac{\left(y_{2s}-y_{1s}\right)}{L_B}y_{1d}-\sin\theta_{Bs}K_{Bd}\frac{\left(y_{2s}-y_{1s}\right)}{L_B}y_{2d}=0\end{aligned} \tag{89}$$

4.3. Translational motion in the y-direction

4.3.1. Equation of Surging Motion of Platform

The dynamic equilibrium of the floating platform in the surging motion is

$$-\left(M_1+m_{eff,y}\right)\ddot{y}_{1d}+f_{py}-\left[T_{A1}\cos\theta_{A1}\cos\left(\Delta_1+\phi_{cur}\right)+T_{A2}\cos\theta_{A2}\cos\Delta_2\right]+T_B\cos\theta_B=0 \tag{90}$$

where the effective mass $m_{eff,y}$ is derived in Appendix A. The hydrodynamic force

$$f_{\mathrm{Py}}=f_{pys}+f_{pyd} \tag{91}$$

where $f_{Pys}=f_{Py}\left(V,0,0,0,0,0,0,0,0,0\right)=C_{DPy}\frac{1}{2}\rho A_{PY}V^2$, $f_{pyd}=\sum_{j=1}^{9}\frac{\partial f_{Py}}{\partial s_{1j}}s_{1j}$. (91)

Substituting Equations (23, 85-87, 91) into Equation (90), one obtains

$$\begin{aligned}&\left(M_1+m_{eff,y}\right)\ddot{y}_{1d}-\left(\frac{\partial f_{Py}}{\partial\dot{x}_{1d}}\dot{x}_{1d}+\frac{\partial f_{Py}}{\partial\dot{y}_{1d}}\dot{y}_{1d}+\frac{\partial f_{Py}}{\partial\dot{z}_{1d}}\dot{z}_{1d}+\frac{\partial f_{Py}}{\partial\dot{\varphi}_{px}}\dot{\varphi}_{px}+\frac{\partial f_{Py}}{\partial\dot{\varphi}_{py}}\dot{\varphi}_{py}+\frac{\partial f_{Py}}{\partial\dot{\varphi}_{pz}}\dot{\varphi}_{pz}\right)\\&-\left(\frac{\partial f_{Py}}{\partial\varphi_{px}}\varphi_{px}+\frac{\partial f_{Py}}{\partial\varphi_{py}}\varphi_{py}+\frac{\partial f_{Py}}{\partial\varphi_{pz}}\varphi_{pz}\right)-\left(d_1+d_2K_{Ad}\varepsilon_{AX}-K_{Bd}X_B\cos\theta_{Bs}\right)x_{1d}\\&-\left(d_3+K_{Bd}X_B\cos\theta_{Bs}\right)x_{2d}-\left(d_2K_{Ad}\varepsilon_{AY}-K_{Bd}Y_B\cos\theta_{Bs}\right)y_{1d}-K_{Bd}Y_B\cos\theta_{Bs}y_{2d}\\&-\left(d_2K_{Ad}\varepsilon_{AZ}-K_{Bd}Z_B\cos\theta_{Bs}\right)z_{1d}-K_{Bd}Z_B\cos\theta_{Bs}z_{2d}=0\end{aligned} \tag{92}$$

where

 doi:10.20944/preprints202407.1940.v1

$$d_1 = T_{As}\left[\frac{\sin\theta_{As1}\cos\left(\Delta_1+\phi_{cur}\right)}{L_{A1}}+\frac{\sin\theta_{As2}\cos\Delta_2}{L_{A2}}\right]-\frac{T_{Bs}\sin\theta_{Bs}}{L_B},$$

$$d_2 = -\left[\cos\theta_{As1}\cos\left(\Delta_1+\phi_{cur}\right)+\cos\theta_{As2}\cos\Delta_2\right], \qquad d_3 = -\frac{T_{Bs}\sin\theta_{Bs}}{L_B}.$$

4.3.2. Equation of Surging Motion of Convertor in the y-direction

The dynamic equilibrium of the convertor in the surging motion is

$$-M_2\ddot{y}_{2d}+f_{Ty}-T_B\cos\theta_B=0 \tag{93}$$

The hydrodynamic force on the convertor is expressed as

$$f_{Ty}=f_{Tys}+f_{Tyd} \tag{94}$$

where $f_{Tys}=f_{Ty}\left(V,0,0,0,0,0,0,0,0,0,TRS\right)=C_{DTy}\frac{1}{2}\rho A_{TY}V^2$, A_{Ty} is the effective operating area of the convertor. $f_{Tyd}=\sum_{j=1}^{9}\frac{\partial f_{Ty}}{\partial s_{2j}}s_{2j}$.

Substituting Equations (85, 87, 94) into Equation (93), one obtains

$$\begin{aligned}M_2\ddot{y}_{2d}&-\left(\frac{\partial f_{Tx}}{\partial\dot{x}_{2d}}\dot{x}_{2d}+\frac{\partial f_{Tx}}{\partial\dot{y}_{2d}}\dot{y}_{2d}+\frac{\partial f_{Tx}}{\partial\dot{z}_{2d}}\dot{z}_{2d}+\frac{\partial f_{Tx}}{\partial\dot{\varphi}_{Tx}}\dot{\varphi}_{Tx}+\frac{\partial f_{Tx}}{\partial\dot{\varphi}_{Ty}}\dot{\varphi}_{Ty}+\frac{\partial f_{Tx}}{\partial\dot{\varphi}_{Tz}}\dot{\varphi}_{Tz}\right)\\&-\left(\frac{\partial f_{Tx}}{\partial\varphi_{Tx}}\varphi_{Tx}+\frac{\partial f_{Tx}}{\partial\varphi_{Ty}}\varphi_{Ty}+\frac{\partial f_{Tx}}{\partial\varphi_{Tz}}\varphi_{Tz}\right)\\&+K_{Bd}\cos\theta_{Bs}\left[-X_Bx_{1d}+X_Bx_{2d}-Y_By_{1d}+Y_By_{2d}-Z_Bz_{1d}+Z_Bz_{2d}\right]=0\end{aligned} \tag{95}$$

4.3.3. Equation of Surging Motion of Pontoon 3 in the y-direction

The dynamic equilibrium of the pontoon 3 in the surging motion is

$$M_3\ddot{y}_{3d}+\frac{T_{Cs}}{L_C}\left(y_{3d}-y_{1d}\right)=0 \tag{96}$$

4.3.4. Equation of Surging Motion of Pontoon 4 in the y-direction

The dynamic equilibrium of the pontoon 4 in the surging motion is

$$M_4\ddot{y}_{4d}+\frac{T_{Ds}}{L_D}\left(y_{4d}-y_{2d}\right)=0 \tag{97}$$

4.4. Translational motion in the z-direction

4.4.1. Equation of Swaying Motion of Platform

The dynamic equilibrium of the floating platform in the swaying motion is

$$\begin{aligned}\left(M_1+m_{eff,z}\right)\ddot{z}_{1d}-f_{Pz}-\left[T_{A1}\cos\theta_{A1}\sin\left(\Delta_1+\phi_{cur}\right)-T_{A2}\cos\theta_{A2}\sin\Delta_2\right]\\-T_B\cos\theta_B\left(\sin\phi_B\right)-T_C\sin\phi_C=0\end{aligned} \tag{98}$$

where the effective mass $m_{eff,z}$ is derived in Appendix A. The hydrodynamic force

$$f_{Pz}=\sum_{j=1}^{9}\frac{\partial f_{Pz}}{\partial s_{1j}}s_{1j}. \tag{99}$$

Considering small displacements and based on Equations (79, 85-87, 99), one obtains

 doi:10.20944/preprints202407.1940.v1

$$\left(M_1+m_{eff,z}\right)\ddot{z}_{1d}-\left(\frac{\partial f_{Pz}}{\partial \dot{x}_{1d}}\dot{x}_{1d}+\frac{\partial f_{Pz}}{\partial \dot{y}_{1d}}\dot{y}_{1d}+\frac{\partial f_{Pz}}{\partial \dot{z}_{1d}}\dot{z}_{1d}+\frac{\partial f_{Pz}}{\partial \dot{\varphi}_{px}}\dot{\varphi}_{px}+\frac{\partial f_{Pz}}{\partial \dot{\varphi}_{py}}\dot{\varphi}_{py}+\frac{\partial f_{Pz}}{\partial \dot{\varphi}_{pz}}\dot{\varphi}_{pz}\right)$$
$$-\frac{\partial f_{Pz}}{\partial \varphi_{px}}\varphi_{px}-\frac{\partial f_{Pz}}{\partial \varphi_{py}}\varphi_{py}-\frac{\partial f_{Pz}}{\partial \varphi_{pz}}\varphi_{pz}+\frac{T_{As}}{L_A}\left(\frac{\sin\theta_{As1}\sin\left(\Delta_1+\phi\right)}{r_{A1}}-\frac{\sin\theta_{As2}\sin\Delta_2}{r_{A2}}\right)x_{1d}$$
$$+\left(\frac{T_{Bs}}{L_B}+\frac{T_{Cs}}{L_C}\right)z_{1d}-\frac{T_{Bs}}{L_B}z_{2d}-\frac{T_{Cs}}{L_C}z_{3d}=0 \quad (100)$$

4.4.2. Equation of Swaying Motion of Convertor

The dynamic equilibrium of the convertor in the swaying motion is

$$M_2\ddot{z}_{2d}-\left(\sum_{j=1}^{3}\frac{\partial f_{Tz}}{\partial s_{2j}}s_{2j}+\sum_{j=7}^{9}\frac{\partial f_{Tz}}{\partial s_{2j}}s_{2j}\right)-\sum_{j=4}^{6}\frac{\partial f_{Tz}}{\partial s_{2j}}s_{2j}-\frac{T_{Bs}}{L_B}z_{1d}+\left(\frac{T_{Bs}}{L_B}+\frac{T_{Ds}}{L_D}\right)z_{2d}-\frac{T_{Ds}}{L_D}z_{4d}=0 \quad (101)$$

4.4.3. Equation of Swaying Motion for Pontoon 3

The dynamic equilibrium of the pontoon 3 in the swaying motion is [8]

$$M_3\ddot{z}_{3d}+\frac{T_{Cs}}{L_C}\left(z_{3d}-z_{1d}\right)=0 \quad (102)$$

4.4.4. Equation of Swaying Motion of Pontoon 4

The dynamic equilibrium of the pontoon 4 in the swaying motion is [8]

$$M_4\ddot{z}_{4d}+\frac{T_{Ds}}{L_D}\left(z_{4d}-z_{2d}\right)=0 \quad (103)$$

4.5. Rotational motion

4.5.1. Equation of Yawing Motion of Convertor

The dynamic equilibrium of the convertor in the yawing motion is [8]

$$I_{Tx}\ddot{\varphi}_{2x}-\left(\sum_{j=1}^{3}\frac{\partial m_{Tx}}{\partial s_{2j}}s_{2j}+\sum_{j=7}^{9}\frac{\partial m_{Tx}}{\partial s_{2j}}s_{2j}\right)-\sum_{j=4}^{6}\frac{\partial m_{Tx}}{\partial s_{2j}}s_{2j}+\left(T_{Bs}\cos\theta_{Bs}R_{TBx}\right)\varphi_{2x}$$
$$-\left(\frac{T_{Bs}R_{TBx}}{L_B}\right)z_{1d}+\left(\frac{T_{Bs}R_{TBx}}{L_B}\right)z_{2d}=0 \quad (104)$$

4.5.2. Equation of Rolling Motion of Convertor

The dynamic equilibrium of the convertor in the rolling motion is [8]

$$I_y\ddot{\varphi}_{2y}-\left(\sum_{j=1}^{3}\frac{\partial m_{Ty}}{\partial s_{2j}}s_{2j}+\sum_{j=7}^{9}\frac{\partial m_{Ty}}{\partial s_{2j}}s_{2j}\right)-\sum_{j=4}^{6}\frac{\partial m_{Ty}}{\partial s_{2j}}s_{2j}+T_{Ds}R_{TDy}\varphi_{2y}+\frac{T_{Ds}R_{TDy}}{L_D}z_{2d}-\frac{T_{Ds}R_{TDy}}{L_D}z_{4d}=0 \quad (105)$$

4.5.3. Equation of Pitching Motion of Convertor

The dynamic equilibrium of the convertor in the pitching motion is [8]

$$I_{Tz}\ddot{\varphi}_{2z}-\left(\sum_{j=1}^{3}\frac{\partial m_{Tyd}}{\partial s_{2j}}s_{2j}+\sum_{j=7}^{9}\frac{\partial m_{Tyd}}{\partial s_{2j}}s_{2j}\right)-\sum_{j=4}^{6}\frac{\partial m_{Tyd}}{\partial s_{2j}}s_{2j}+\left(T_{Bs}R_{TBz}\cos\theta_B\right)\varphi_{2z}$$
$$-\frac{T_{Bs}R_{TBz}\cos\theta_B}{L_B}x_{1d}+\frac{T_{Bs}R_{TBz}\cos\theta_B}{L_B}x_{2d}=0 \quad (106)$$

4.5.4. Equation of Yawing Motion of Platform

 doi:10.20944/preprints202407.1940.v1

The dynamic equilibrium of the floating platform in the yawing motion is

$$I_{Px}\ddot{\varphi}_{Px}-m_{Px}+T_A R_{PAx}\left[\cos\left(\theta_{A1s}+\Delta\theta_{A1}\right)\sin\left(\varphi_{Px}-\Delta\phi_{x1}\right)+\cos\left(\theta_{A2s}+\Delta\theta_{A2}\right)\sin\left(\varphi_{Px}-\Delta\phi_{x2}\right)\right]$$
$$+T_B\cos\left(\theta_{Bs}+\Delta\theta_B\right)R_{PBx}\sin\left(\varphi_{Px}-\Delta\theta_x\right)=0 \tag{107}$$

where $\Delta\phi_{x1}=\dfrac{z_{1d}}{L_{A1}\cos\theta_{A1s}},\Delta\phi_{x2}=\dfrac{z_{1d}}{L_{A2}\cos\theta_{A2s}}$, $\Delta\theta_x=\dfrac{z_{2d}-z_{1d}}{L_B\cos\theta_{Bs}}$. Substituting Equations (85-87) and hydrodynamic moment m_{px} into Equation (107), one obtains

$$I_{Px}\ddot{\varphi}_{Px}-\left(\frac{\partial m_{Px}}{\partial\dot{x}_{1d}}\dot{x}_{1d}+\frac{\partial m_{Px}}{\partial\dot{y}_{1d}}\dot{y}_{1d}+\frac{\partial m_{Px}}{\partial\dot{z}_{1d}}\dot{z}_{1d}+\frac{\partial m_{Px}}{\partial\dot{\varphi}_{Px}}\dot{\varphi}_{Px}+\frac{\partial m_{Px}}{\partial\dot{\varphi}_{Py}}\dot{\varphi}_{Py}+\frac{\partial m_{Px}}{\partial\dot{\varphi}_{Pz}}\dot{\varphi}_{Pz}\right)$$
$$+\left(T_{As}R_{PAx}\left(\cos\theta_{A1s}+\cos\theta_{A2s}\right)+T_{Bs}\cos\theta_{Bs}R_{PBx}-\frac{\partial m_{Px}}{\partial\varphi_{px}}\right)\varphi_{Px}-\frac{\partial m_{Px}}{\partial\varphi_{Py}}\varphi_{Py}-\frac{\partial m_{Px}}{\partial\varphi_{Pz}}\varphi_{Pz}$$
$$+\left(\frac{T_{Bs}R_{PBx}}{L_B}-T_{As}R_{PAx}\left(\frac{1}{L_{A1}}+\frac{1}{L_{A2}}\right)\right)z_{1d}-\frac{T_{Bs}R_{PBx}}{L_B}z_{2d}=0 \tag{108}$$

4.5.5. Equation of Rolling Motion of Platform

The dynamic equilibrium of the floating platform in the rolling motion is

$$I_{Py}\ddot{\varphi}_{Py}-m_{Py}+T_A R_{PAy}\left[\cos\left(\theta_{A1s}+\Delta\theta_{A1}\right)\sin\left(\varphi_{Py}+\Delta\phi_{A1y}\right)+\cos\left(\theta_{A2s}+\Delta\theta_{A2}\right)\sin\left(\varphi_{Py}+\Delta\phi_{A2y}\right)\right]$$
$$+T_C R_{PCy}\sin\left(\varphi_{Py}+\Delta\phi_{Cy}\right)=0 \tag{109}$$

where $\Delta\phi_{Cy}=\dfrac{z_{1d}-z_{3d}}{L_C}$, $\Delta\phi_{A1y}=\dfrac{z_{1d}}{L_{A1}\sin\theta_{A1s}}$, $\Delta\phi_{A2y}=\dfrac{z_{1d}}{L_{A2}\sin\theta_{A2s}}$. Substituting Equations (79, 85-86) and hydrodynamic moment m_{py} into Equation (109), one obtains

$$I_{Py}\ddot{\varphi}_{Py}-\left(\frac{\partial m_{Py}}{\partial\dot{x}_{1d}}\dot{x}_{1d}+\frac{\partial m_{Py}}{\partial\dot{y}_{1d}}\dot{y}_{1d}+\frac{\partial m_{Py}}{\partial\dot{z}_{1d}}\dot{z}_{1d}+\frac{\partial m_{Py}}{\partial\dot{\varphi}_{Px}}\dot{\varphi}_{Px}+\frac{\partial m_{Py}}{\partial\dot{\varphi}_{Py}}\dot{\varphi}_{Py}+\frac{\partial m_{Py}}{\partial\dot{\varphi}_{Pz}}\dot{\varphi}_{Pz}\right)$$
$$-\frac{\partial m_{Py}}{\partial\varphi_{px}}\varphi_{px}+\left[T_{As}R_{PAy}\left(\cos\theta_{A1s}+\cos\theta_{A2s}\right)+T_{Cs}R_{PCy}-\frac{\partial m_{Py}}{\partial\varphi_{Py}}\right]\varphi_{Py}-\frac{\partial m_{Py}}{\partial\varphi_{Pz}}\varphi_{Pz}$$
$$+\left(T_{As}R_{PAy}\left(\frac{1}{L_{A1}}+\frac{1}{L_{A2}}\right)+\frac{T_{Cs}R_{PCy}}{L_C}\right)z_{1d}-\frac{T_{Cs}R_{PCy}}{L_C}z_{3d}=0 \tag{110}$$

4.5.6. Equation of Pitching Motion of Platform

The dynamic pitching equilibrium of the floating platform about the z-axis is

$$I_{Pz}\ddot{\varphi}_{Pz}-m_{Pz}+T_A R_{PAz}\left[\cos\left(\theta_{As1}+\Delta\theta_{A1}\right)\sin\left(\varphi_{Pz}+\Delta\theta_{A1}\right)+\cos\left(\theta_{As2}+\Delta\theta_{A2}\right)\sin\left(\varphi_{Pz}+\Delta\theta_{A2}\right)\right]$$
$$+T_B\cos\left(\theta_{Bs}+\Delta\theta_B\right)R_{PBz}\sin\left(\varphi_{Pz}+\Delta\theta_B\right)+T_C R_{PCz}\sin\left(\varphi_{Pz}+\Delta\theta_C\right)=0 \tag{111}$$

where $\Delta\theta_{A1}=\dfrac{x_{1d}}{L_{A1}}$, $\Delta\theta_{A2}=\dfrac{x_{1d}}{L_{A2}}$, $\Delta\theta_B=\dfrac{x_{2d}-x_{1d}}{L_B}$, $\Delta\theta_C=\dfrac{y_{2d}-y_{1d}}{L_C}$. Substituting Equations (79, 85-86) and hydrodynamic moment m_{py} into Equation (111), one obtains

$$I_{Pz}\ddot{\varphi}_{Pz}-\left(\frac{\partial m_{Pz}}{\partial\dot{x}_{1d}}\dot{x}_{1d}+\frac{\partial m_{Pz}}{\partial\dot{y}_{1d}}\dot{y}_{1d}+\frac{\partial m_{Pz}}{\partial\dot{z}_{1d}}\dot{z}_{1d}+\frac{\partial m_{Pz}}{\partial\dot{\varphi}_{Px}}\dot{\varphi}_{Px}+\frac{\partial m_{Pz}}{\partial\dot{\varphi}_{Py}}\dot{\varphi}_{Py}+\frac{\partial m_{Pz}}{\partial\dot{\varphi}_{Pz}}\dot{\varphi}_{Pz}\right)$$
$$-\frac{\partial m_{Pz}}{\partial\varphi_{px}}\varphi_{px}-\frac{\partial m_{Pz}}{\partial\varphi_{Py}}\varphi_{Py}+\left(T_{As}R_{PAz}\left(\cos\theta_{A1s}+\cos\theta_{A2s}\right)+T_{Bs}\cos\theta_{Bs}R_{PBz}+T_{Cs}R_{PCz}-\frac{\partial m_{Pz}}{\partial\varphi_{Pz}}\right)\varphi_{Pz}$$
$$+\left(T_{As}R_{PAz}\left(\frac{\cos\theta_{A1s}}{L_{A1}}+\frac{\cos\theta_{A2s}}{L_{A2}}\right)-\frac{T_{Bs}\cos\theta_{Bs}R_{PBz}}{L_B}\right)x_{1d}$$
$$+\frac{T_{Bs}\cos\theta_{Bs}R_{PBz}}{L_B}x_{2d}+\frac{T_{Cs}R_{PCz}}{L_C}\left(y_{2d}-y_{1d}\right)=0 \tag{112}$$

 doi:10.20944/preprints202407.1940.v1

4.6. Solution Method of Dynamic Displacements

The governing equations (77, 80, 88-89, 92-97, 100-106, 108, 110, 112) can be expressed in matrix format

$$\mathbf{M}\ddot{\mathbf{Z}}_d + \mathbf{C}\dot{\mathbf{Z}}_d + \mathbf{K}\mathbf{Z}_d = \mathbf{F}_d \quad (113)$$

where the dynamic displacement vector $\mathbf{Z}_d = \left[x_{1d}\ y_{1d}\ z_{1d}\ x_{2d}\ y_{2d}\ z_{2d}\ x_{3d}\ y_{3d}\ z_{3d}\ x_{4d}\ y_{4d}\ z_{4d}\ \varphi_{Tx}\ \varphi_{Ty}\ \varphi_{Tz}\ \varphi_{Px}\ \varphi_{Py}\ \varphi_{Pz}\right]^T$.

The elements of the force vector

$$\mathbf{F_d} = \left[0\ 0\ 0\ 0\ 0\ 0\ f_7\ 0\ 0\ 0\ f_{10}\ 0\ 0\ 0\ 0\ 0\ 0\ 0\right]^T_{18\times 1} \quad (114)$$

where

$$f_7 = \sum_{i=1}^{N}\left[f_{Bs,i}\sin\Omega_i t + f_{Bc,i}\cos\Omega_i t\right], \quad f_{10} = \sum_{i=1}^{N}\left[f_{Ts,i}\sin\Omega_i t + f_{Tc,i}\cos\Omega_i t\right],$$
$$f_{Bs,i} = A_{Bx}\rho g a_i\cos\varphi_i, \quad f_{Bc,i} = A_{Bx}\rho g a_i\sin\varphi_i,$$
$$f_{Ts,i} = A_{BT}\rho g a_i\cos\left(\varphi_i+\phi_i\right), \quad f_{Tc,i} = A_{BT}\rho g a_i\sin\left(\varphi_i+\phi_i\right). \quad (115)$$

According to the FSI parameters of 400kW convertor and platform presented by Lin *et al*. [8] and considering the similarity of some prototype of different power, for example, 1 MW. The elements of the mass matrix $\mathbf{M} = \left[M_{ij}\right]_{18\times 18}$, the damping matrix $\mathbf{C} = \left[C_{ij}\right]_{18\times 18}$ and the stiffness matrix $\mathbf{K} = \left[K_{ij}\right]_{18\times 18}$ for the prototype of MW-level are determined by using the similar formula in section 4-1 and listed in Appendix *B*, *C* and *D*, respectively. Equation (113) can be rewritten as

$$\ddot{\mathbf{Z}}_d + \mathbf{M}^{-1}\mathbf{C}\dot{\mathbf{Z}}_d + \mathbf{M}^{-1}\mathbf{K}\mathbf{Z}_d = \mathbf{M}^{-1}\mathbf{F}_d = \sum_{i=1}^{N}\left(\mathbf{F}_{s,i}\sin\Omega_i t + \mathbf{F}_{c,i}\cos\Omega_i t\right) \quad (116)$$

where

$$\mathbf{F}_{s,i} = \left[0\ \ 0\ \ 0\ \ 0\ \ 0\ \ 0\ \ \frac{f_{Bs,i}}{M_{77}}\ \ 0\ \ 0\ \ 0\ \ \frac{f_{Ts,i}}{M_{1010}}\ \ 0\ \ 0\ \ 0\ \ 0\ \ 0\ \ 0\ \ 0\right]^T,$$
$$\mathbf{F}_{c,i} = \left[0\ \ 0\ \ 0\ \ 0\ \ 0\ \ 0\ \ \frac{f_{Bc,i}}{M_{77}}\ \ 0\ \ 0\ \ 0\ \ \frac{f_{Tc,i}}{M_{1010}}\ \ 0\ \ 0\ \ 0\ \ 0\ \ 0\ \ 0\ \ 0\right]. \quad (117)$$

The solution can be expressed as

$$\mathbf{Z}_d = \left[x_{1d}\ y_{1d}\ z_{1d}\ x_{2d}\ y_{2d}\ z_{2d}\ x_{3d}\ y_{3d}\ z_{3d}\ x_{4d}\ y_{4d}\ z_{4d}\ \varphi_{Tx}\ \varphi_{Ty}\ \varphi_{Tz}\ \varphi_{Px}\ \varphi_{Py}\ \varphi_{Pz}\right]^T$$
$$= \sum_{i=1}^{N}\left(\mathbf{Z}_{\mathbf{d}c,i}\cos\Omega_i t + \mathbf{Z}_{\mathbf{d}s,i}\sin\Omega_i t\right) \quad (118)$$

where

$$\mathbf{Z}_{dc,i} = \left[x_{1dc,i}\ y_{1dc,i}\ z_{1dc,i}\ x_{2dc,i}\ y_{2dc,i}\ z_{2dc,i}\ x_{3dc,i}\ y_{3dc,i}\ z_{3dc,i}\ x_{4dc,i}\ y_{4dc,i}\ z_{4dc,i}\ \varphi_{Txc,i}\ \varphi_{Tyc,i}\ \varphi_{Tzc,i}\ \varphi_{Pxc,i}\ \varphi_{Pyc,i}\ \varphi_{Pzc,i}\right]^T,$$
$$\mathbf{Z}_{ds,i} = \left[x_{1ds,i}\ y_{1ds,i}\ z_{1ds,i}\ x_{2ds,i}\ y_{2ds,i}\ z_{2ds,i}\ x_{3ds,i}\ y_{3ds,i}\ z_{3ds,i}\ x_{4ds,i}\ y_{4ds,i}\ z_{4ds,i}\ \varphi_{Txs,i}\ \varphi_{Tys,i}\ \varphi_{Tzs,i}\ \varphi_{Pxs,i}\ \varphi_{Pys,i}\ \varphi_{Pzs,i}\right]^T \quad (119)$$

Substituting the solution (118) into Equation (116), one obtains

$$-\sum_{i=1}^{N}\Omega_i^2\left(\mathbf{Z}_{\mathbf{d}c,i}\cos\Omega_i t + \mathbf{Z}_{\mathbf{d}s,i}\sin\Omega_i t\right) + \mathbf{M}^{-1}\mathbf{C}\sum_{i=1}^{N}\left(-\Omega_i\mathbf{Z}_{\mathbf{d}c,i}\sin\Omega_i t + \Omega_i\mathbf{Z}_{\mathbf{d}s,i}\cos\Omega_i t\right)$$
$$+\mathbf{M}^{-1}\mathbf{K}\sum_{i=1}^{N}\left(\mathbf{Z}_{\mathbf{d}c,i}\cos\Omega_i t + \mathbf{Z}_{\mathbf{d}s,i}\sin\Omega_i t\right) = \sum_{i=1}^{N}\left(\mathbf{F}_{s,i}\sin\Omega_i t + \mathbf{F}_{c,i}\cos\Omega_i t\right) \quad (120)$$

By using the balanced method for Equation (120), one obtains

$$\sum_{i=1}^{N}\mathbf{a}_{im}\mathbf{Z}_{\mathbf{d}c,i} + \sum_{i=1}^{N}\mathbf{b}_{im}\mathbf{Z}_{\mathbf{d}s,i} = \boldsymbol{\chi}_{cm},\quad m = 1,2,\ldots,N \quad (121)$$

 doi:10.20944/preprints202407.1940.v1

where $\mathbf{a}_{im}=\left[\alpha_{im}\left(\mathbf{M}^{-1}\mathbf{K}-\Omega_i^2\mathrm{I}\right)-\beta_{im}\Omega_i\mathbf{M}^{-1}\mathbf{C}\right]$, $\mathbf{b}_{im}=\left[\beta_{im}\left(\mathbf{M}^{-1}\mathbf{K}-\Omega_i^2\mathrm{I}\right)-\alpha_{im}\Omega_i\mathbf{M}^{-1}\mathbf{C}\right]$,

$\boldsymbol{\chi}_{cm}=\sum_{i=1}^{N}\left(\mathbf{F}_{s,i}\beta_{im}+\mathbf{F}_{c,i}\alpha_{im}\right)$.

and

$$\sum_{i=1}^{N}\mathbf{c}_{im}\mathbf{Z}_{\mathbf{d}c,i}+\sum_{i=1}^{N}\mathbf{d}_{im}\mathbf{Z}_{\mathbf{d}s,i}=\boldsymbol{\chi}_{sm},\quad m=1,2,...,N=6 \tag{122}$$

where $\mathbf{c}_{im}=\left[\beta_{mi}\left(\mathbf{M}^{-1}\mathbf{K}-\Omega_i^2\mathrm{I}\right)-\gamma_{im}\Omega_i\mathbf{M}^{-1}\mathbf{C}\right]$, $\mathbf{d}_{im}=\left[\gamma_{im}\left(\mathbf{M}^{-1}\mathbf{K}-\Omega_i^2\mathrm{I}\right)-\beta_{mi}\Omega_i\mathbf{M}^{-1}\mathbf{C}\right]$, and

$\boldsymbol{\chi}_{sm}=\sum_{i=1}^{N}\left(\mathbf{F}_{s,i}\gamma_{im}+\mathbf{F}_{c,i}\beta_{mi}\right)$.

Equations (121-122) can be expressed as

$$\mathbf{A}\tilde{\mathbf{Z}}_d=\mathbf{F} \tag{123}$$

where

$$\mathbf{A}=\begin{bmatrix}\begin{bmatrix}\mathbf{a}_{11} & \mathbf{a}_{21} & \cdots & \mathbf{a}_{\mathrm{N},1}\\ \mathbf{a}_{12} & \mathbf{a}_{22} & \cdots & \mathbf{a}_{\mathrm{N}2}\\ \vdots & \vdots & \cdots & \vdots\\ \mathbf{a}_{1\mathrm{N}} & \mathbf{a}_{2N} & \cdots & \mathbf{a}_{\mathrm{NN}}\end{bmatrix}_{18\mathrm{N}\times18\mathrm{N}} & \begin{bmatrix}\mathbf{b}_{11} & \mathbf{b}_{21} & \cdots & \mathbf{b}_{N1}\\ \mathbf{b}_{12} & \mathbf{b}_{22} & \cdots & \mathbf{b}_{N2}\\ \vdots & \vdots & \cdots & \vdots\\ \mathbf{b}_{1,N} & \mathbf{b}_{2,N} & \cdots & \mathbf{b}_{NN}\end{bmatrix}_{18\mathrm{N}\times18\mathrm{N}}\\ \begin{bmatrix}\mathbf{c}_{11} & \mathbf{c}_{21} & \cdots & \mathbf{c}_{N1}\\ \mathbf{c}_{12} & \mathbf{c}_{22} & \cdots & \mathbf{c}_{N2}\\ \vdots & \vdots & \cdots & \vdots\\ \mathbf{c}_{1N} & \mathbf{c}_{2N} & \cdots & \mathbf{c}_{\mathrm{NN}}\end{bmatrix}_{18\mathrm{N}\times18\mathrm{N}} & \begin{bmatrix}\mathbf{d}_{11} & \mathbf{d}_{21} & \cdots & \mathbf{d}_{N1}\\ \mathbf{d}_{12} & \mathbf{d}_{22} & \cdots & \mathbf{d}_{N2}\\ \vdots & \vdots & \cdots & \vdots\\ \mathbf{d}_{1N} & \mathbf{d}_{2N} & \cdots & \mathbf{d}_{\mathrm{NN}}\end{bmatrix}_{18\mathrm{N}\times18\mathrm{N}}\end{bmatrix}_{36\mathrm{N}\times36\mathrm{N}}$$

$$\tilde{\mathbf{Z}}_d=\begin{bmatrix}\begin{bmatrix}\mathbf{z}_{\mathbf{d}c,1}\\ \mathbf{z}_{\mathbf{d}c,2}\\ \vdots\\ \mathbf{z}_{\mathbf{d}c,N=6}\end{bmatrix}_{18\mathrm{N}\times1}\\ \begin{bmatrix}\mathbf{z}_{\mathbf{d}s,1}\\ \mathbf{z}_{\mathbf{d}s,2}\\ \vdots\\ \mathbf{z}_{\mathbf{d}s,N=6}\end{bmatrix}_{18\mathrm{N}\times1}\end{bmatrix}_{36\mathrm{N}\times1},\quad \mathbf{F}=\begin{bmatrix}\begin{bmatrix}\boldsymbol{\chi}_{c1}\\ \boldsymbol{\chi}_{c2}\\ \vdots\\ \boldsymbol{\chi}_{c,\mathrm{N}=6}\end{bmatrix}_{18\mathrm{N}\times1}\\ \begin{bmatrix}\boldsymbol{\chi}_{\mathrm{s}1}\\ \boldsymbol{\chi}_{\mathrm{s}2}\\ \vdots\\ \boldsymbol{\chi}_{\mathrm{s},\mathrm{N}=6}\end{bmatrix}_{18\mathrm{N}\times1}\end{bmatrix}_{36\mathrm{N}\times1}. \tag{124}$$

The solution of Equation (123) is

$$\tilde{\mathbf{Z}}_d=\mathbf{A}^{-1}\mathbf{F} \tag{125}$$

4.8. Dynamic Tensions of Ropes

Under irregular wave, the dynamic tension of rope *A* is

$$T_{Ad}=\sum_{i=1}^{N}T_{Adc,i}\cos\Omega_i t+T_{Ads,i}\sin\Omega_i t \tag{126}$$

where $T_{Adc,i}=K_{Ad}\left(\varepsilon_{AX}x_{1dc,i}+\varepsilon_{AY}y_{1dc,i}+\varepsilon_{AZ}z_{1dc,i}\right)$, $T_{Ads,i}=K_{Ad}\left(\varepsilon_{AX}x_{1ds,i}+\varepsilon_{AY}y_{1ds,i}+\varepsilon_{AZ}z_{1ds,i}\right)$. The dynamic tension of rope *B* is

$$T_{Bd}=\sum_{i=1}^{N}T_{Bdc,i}\cos\Omega_i t+T_{Bds,i}\sin\Omega_i t \tag{127}$$

Where $T_{Bdc,i}=K_{Bd}\left[X_B\left(x_{2dc,i}-x_{1dc,i}\right)+Y_B\left(y_{2dc,i}-y_{1dc,i}\right)+Z_B\left(z_{2dc,i}-z_{1dc,i}\right)\right]$,

$T_{Bds,i}=K_{Bd}\left[X_B\left(x_{2ds,i}-x_{1ds,i}\right)+Y_B\left(y_{2ds,i}-y_{1ds,i}\right)+Z_B\left(z_{2ds,i}-z_{1ds,i}\right)\right]$,

Preprints.org (www.preprints.org) | NOT PEER-REVIEWED | Posted: 24 July 2024 doi:10.20944/preprints202407.1940.v1

$$X_B = \frac{(x_{2s} - x_{1s})}{L_B},\ Y_B = \frac{(y_{2s} - y_{1s})}{L_B},\ Z_B = \frac{(z_{2s} - z_{1s})}{L_B}.$$

The dynamic tension of rope *C* is

$$T_{Cd} = \sum_{i=1}^{N} T_{Cdc,i} \cos \Omega_i t + T_{Cds,i} \sin \Omega_i t \quad (128)$$

where $T_{Cdc,i} = K_{Cd}\left(x_{3\mathbf{d}c,i} - x_{1dc,i}\right), T_{Cds,i} = K_{Cd}\left(x_{3\mathbf{d}s,i} - x_{1ds,i}\right)$. The dynamic tension of rope *D* is

$$T_{Dd} = \sum_{i=1}^{N} T_{Ddc,i} \cos \Omega_i t + T_{Dds,i} \sin \Omega_i t \quad (129)$$

where $T_{Ddc,i} = K_{Dd}\left(x_{4\mathbf{d}c,i} - x_{2dc,i}\right), T_{Dds,i} = K_{Dd}\left(x_{4\mathbf{d}s,i} - x_{2ds,i}\right)$.

5. Dynamic Response and Discussion

Referring the information from the Central Meteorological Bureau Library of Taiwan about the typhoon invading Taiwan from 1897 to 2019 [18] and selecting 150 typhoons greatly affecting Taiwan's Green Island, the significant wave height H_s during the 50-year regression period H_s =15.4m, the peak period T_w = 16.5sec. Letting N=6, the irregular wave is simulated by six regular waves listed in Table 2 [19]. Figure 6 demonstrates the relation between the significant height H_s and the amplitudes of six regular simulating waves. Table 2 shows that the second wave frequency is completely consistent with the significant frequency. Figure 5 demonstrates that the amplitude of the second wave is significantly larger than that of other waves. The larger the significant wave height H_s is, greatly the larger the amplitudes of the six regular waves are.

Table 2. Irregular wave simulated by six regular waves (H_{bed}=1300m).

Significant frequency	Parameter	Regular wave					
		1	2	3	4	5	6
T_p =15.0s, f_p =0.067Hz	f_i(Hz)	0.043	0.067	0.092	0.115	0.150	0.267
	k_i(1/m)	0.0073	0.0179	0.0339	0.0533	0.0906	0.2861
	l_i(m)	863.6	350.9	185.6	117.9	69.3	22.0
T_p =16.5s, f_p =0.061Hz	f_i(Hz)	0.043	0.061	0.086	0.115	0.150	0.267
	k_i(1/m)	0.0073	0.0148	0.0295	0.0533	0.0906	0.2861
	l_i(m)	863.6	424.7	212.8	117.9	69.3	22.0
T_p=17.5s, f_p=0.057Hz	f_i(Hz)	0.043	0.057	0.082	0.115	0.150	0.267
	k_i(1/m)	0.0073	0.0132	0.0272	0.0533	0.0906	0.2861
	l_i(m)	863.6	477.6	231.2	117.9	69.3	22.0
	φ_i (°)	30	60	90	120	170	300

 doi:10.20944/preprints202407.1940.v1

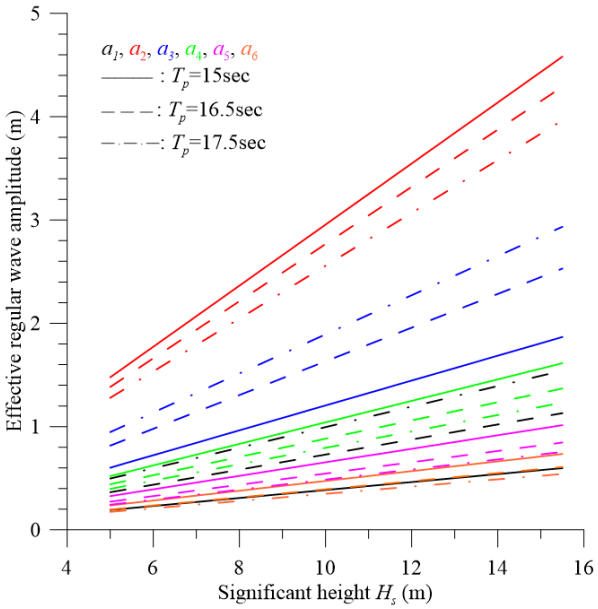

Figure 6. the relation between the significant height H_s and the amplitudes of six regular simulating waves a_i.

The dynamic response of an ocean current convertor of 1 MW power under Typhon irregular wave and current direction is investigated, as shown in Figure 7. The corresponding hydrodynamic coefficients and other parameters are determined based on the similarity law derived in Section 4.1 and listed in Appendix C, D. The parameters of the mooring system are listed in Table 3

Table 3. parameters of the system of 1 MW convertor.

Parameter	Dimension	Parameter	Dimension
depth of seabed H_{bed}	1300m	length of rope A, L_A	5980m
length of rope B, L_B	152.97m	length of rope C, L_C	100m
length of rope D, L_D	70m	distance between two foundations, L_F	1196m
current velocity V	1.5m/s	net buonyance of invertor and platform F_{BNT}/ F_{BNB}	1543.6/689.2tons
static drag of the invertor F_{DT}	148.3 tons	static drag of the platform F_{DB}	0.192 tons
mass of the platform M_1	790.6 tons	mass of the invertor M_2	2126.6 tons
mass of the pontoon 3, M_3	395.3tons	mass of the pontoon 4, M_4	474.3tons
cross-sectional area of surfaced cylinder of pontoon 3, A_{BX}	5.75m²	mass moment of inertia of the convertor about the x, y, z-axis, I_{Tx} / I_{Ty} / I_{Tz}	8.83×10^{11} / 2.68×10^{11} / 8.83×10^{11} $kg-m^2$

 doi:10.20944/preprints202407.1940.v1

cross-sectional area of surfaced cylinder of pontoon 4, A_{BT}		5.75m²	mass moment of inertia of the platform about the x,y,z-axis, I_{Px} / I_{Py} / I_{Pz}	2.96×10^9 / 4.94×10^7 / 2.96×10^9 $kg-m^2$
significant wave height H_s		15.4m	significant period T_p	16.5s
relative angle between current and wave a		30°	phase angles of six regular simulating the irregular wave φ_i	30/60/90/120/170 /300°
HMPE / Dyneema® SK75	Young's modulus E_{PE}	116GPa,	distance from gravities of platform and convertor	R_{TBx}=26.1m R_{TDy} = 20.3m R_{TBz} = 26.1m $R_{PAx}=R_{PAy}=R_{PAz}=7.9m$ $R_{PBx}=R_{PBz}=9.2m$ $R_{PCy}=R_{PCz}=4.0m$
	weight per unit length w_{PE}	24.47kg/m		
	diameter D_{PE}	178.9mm		
	cross sectional area A_{PE}	0.0251m²		
	fracture strength T_{frac}	2000tons		

Figure 7 demonstrates the effects of the distance of two foundations L_F and the current direction φ_{cur} on the maximum rope tensions and the displacements of elements under typhon irregular wave. As shown in Figure 7(a), the effect of the current direction on the maximum dynamic tensions of ropes is great. The maximum dynamic tension of rope D, $T_{D,max}$, is significantly larger than the others. The larger the distance of two foundations is, the larger the maximum dynamic tensions are. As shown in Figure 7(b), the maximum heaving displacements of all the elements are greatest. The surging displacement are next. The swaying displacements are negligible. The effect of the current direction φ_{cur} on displacements is negligible. As shown in Figure 7(c), the pitching angle of the platform φ_{pz} is about 2°. The other angular displacement of platform and turbine are very small.

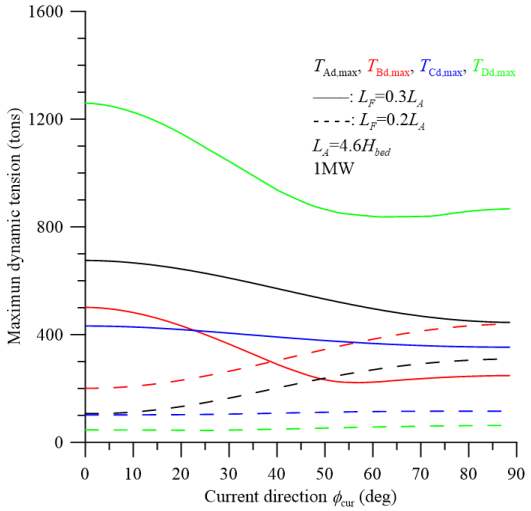

(a)effect of L_F and φ_{cur} on the dynamic tension

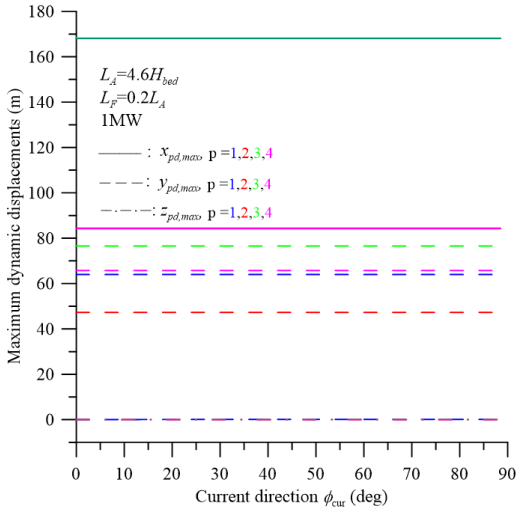

(b)effect of L_F and φ_{cur} on the dynamic displacements

Preprints.org (www.preprints.org) | NOT PEER-REVIEWED | Posted: 24 July 2024 doi:10.20944/preprints202407.1940.v1

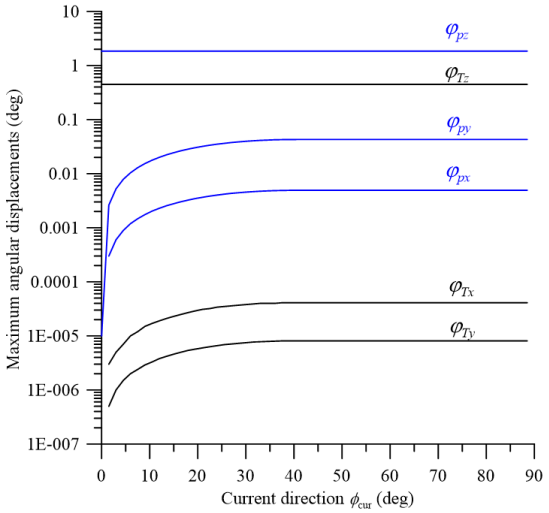

(c) effect of L_F and φ_{cur} on the angular displacements

Figure 7. effects of the distance of two foundations L_F and the current direction φ_{cur} on the maximum rope tensions and the displacements of elements.

Figure 8 demonstrates the comparison of dynamic rope tensions of the traditional mooring system with a single rope A and one with a pulley-rope set under typhoon irregular wave. All the parameters are listed in Table 3. The distance of two foundations L_F=0.2L_A. Figure 8 shows that the dynamic rope tensions of the traditional mooring system with a single rope A are significantly greater than those of the presented one with a pulley- rope set. The dynamic rope tensions $T_{Ad,max}$ and $T_{Bd,max}$ of the traditional system are larger than the fracture strength T_{frac}=2000tons. However, all the dynamic tensions of the pulley- traction rope system is smaller than the fracture strength T_{frac}=2000tons. Obviously, the pulley-rope design can effectively reduce the dynamic rope tensions. For the traditional system, the dynamic tension of rope B is the greatest. However, for the pulley-rope system, the dynamic tension of rope D is the greatest. The dynamic tension of the rope in the traditional system has nothing to do with the current direction $f_{cur,}$ while the dynamic rope tensions of the pulley-rope system is significantly related to the current direction f_{cur}.

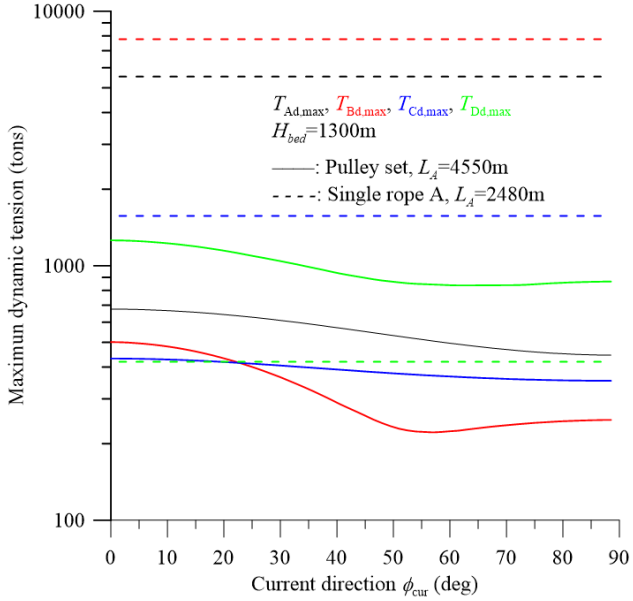

Figure 8. comparison of the dynamic tensions of two mooring systems with a single rope A and a pulley-rope design.

 doi:10.20944/preprints202407.1940.v1

Figure 9 demonstrates the effects of the rope length ratio $r_{AH} = L_A / H_{bed}$ and the current direction φ_{cur} on the dynamic rope tensions of the pulley-rope system of 1 MW under typhoon irregular wave. The distance between two foundations L_F=0.2L_A. Other parameters are the same as those of Table 3. As shown in Figure 9(a), if H_{bed} =1300m, $\varphi_{cur} = 0^o$, $3.98 < r_{AH} < 4.68$, the maximum dynamic tensions $T_{Dd,max}$ is smaller than the fracture strength T_{frac}=2000tons. If H_{bed} =1300m, $\varphi_{cur} = 60^o$, $4.06 < r_{AH} < 4.78$, the maximum dynamic tensions $T_{Dd,max}$ is smaller than the fracture strength T_{frac}=2000tons. As shown in Figure 9(b), if H_{bed} =1000m, $\varphi_{cur} = 0^o$, $3.92 < r_{AH} < 4.39$, the maximum dynamic tensions $T_{Dd,max}$ is smaller than the fracture strength T_{frac}=2000tons. If H_{bed} =1000m, $\varphi_{cur} = 60^o$, $3.99 < r_{AH} < 4.51$, the maximum dynamic tensions $T_{Dd,max}$ is smaller than the fracture strength T_{frac}=2000tons. It is concluded that for a convertor of 1 MW power and H_{bed} =1300m, the rope length ratio, $4.1 \le r_{AH} \le 4.6$, all the dynamic tensions can be smaller than the fracture strength. If H_{bed} =1000m, the rope length ratio, $4.0 \le r_{AH} \le 4.3$, all the dynamic tensions can be smaller than the fracture strength.

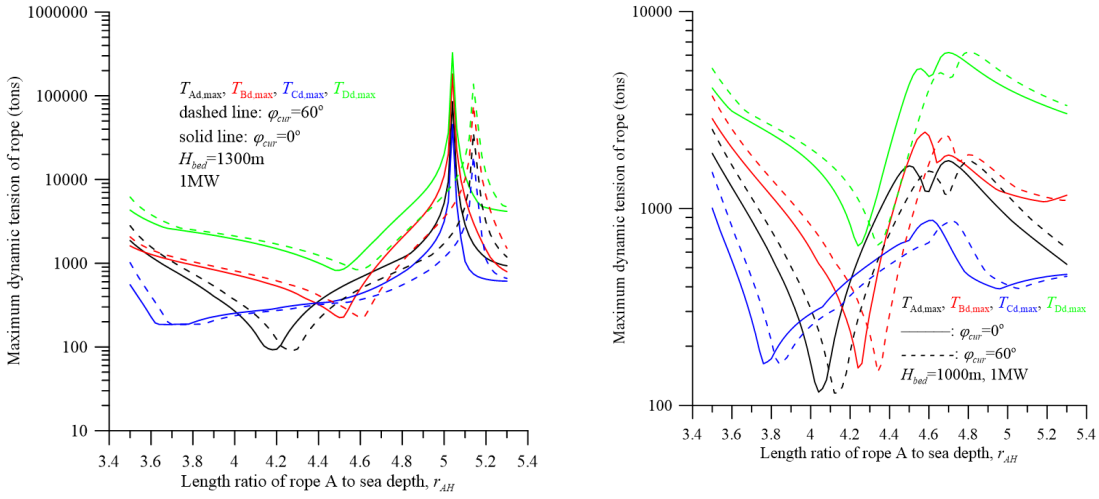

(a) H_{bed}=1300m (b) H_{bed}=1000m

Figure 9. effects of the length of rope A, L_A and the current direction φ_{cur} on the maximum rope tensions.

Figure 10a demonstrates the effects of the buffer spring constant g_{KB} and the current direction φ_{cur} on the dynamic rope tensions of the pulley-rope system of 1 MW under typhoon irregular wave. The buffer springs A, C, and D are not installed. The distance between two foundations L_F=0.2L_A. Other parameters are the same as those of Table 3. It is found that if the buffer spring constant g_{KB}<30, the maximum dynamic tensions are greater than the fracture strength of rope T_{frac}=2000tons.

When the buffer spring constant g_{KB}>100, i.e., the buffer spring B is not installed, the maximum dynamic tension $T_{Dd,max}$ ($\varphi_{cur} = 0^o$)=1259 tons, $T_{Dd,max}$ ($\varphi_{cur} = 60^o$)=839 tons are both less than the fracture strength 2000tons. Figure 10b demonstrates the effects of the buffer spring constant g_{KD} and the current direction φ_{cur} on the dynamic rope tensions of the pulley-rope system of 1 MW under typhoon irregular wave. The buffer springs A, B, and C are not installed. The distance between two foundations L_F=0.2L_A. Other parameters are the same as those of Table 3. It is found that if the buffer spring constant g_{KD}<4.6, the maximum dynamic tensions are greater than the fracture strength of rope T_{frac}=2000tons. When the buffer spring constant g_{KD}>100, i.e., the buffer spring D is not installed, the maximum dynamic tension $T_{Dd,max}$ ($\varphi_{cur} = 0^o$)=1259 tons, $T_{Dd,max}$ ($\varphi_{cur} = 60^o$)=839 tons are both less than the fracture strength 2000tons. It is concluded that the pulley-rope system of 1 MW without the buffer springs A, B, C, and D under the typhoon irregular wave is safety.

Preprints.org (www.preprints.org) | NOT PEER-REVIEWED | Posted: 24 July 2024 doi:10.20944/preprints202407.1940.v1

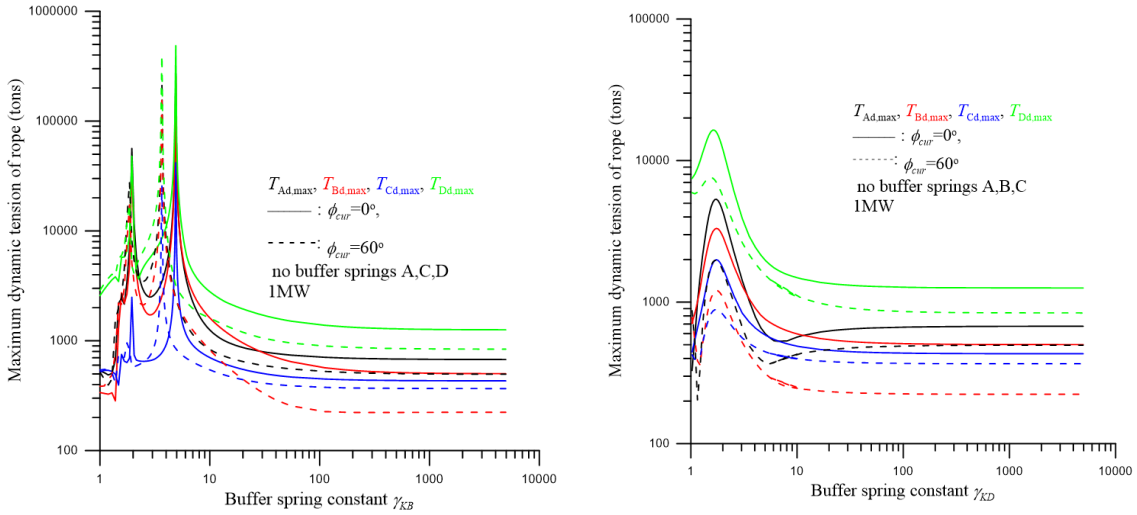

(a) effect of buffer spring B (b) effect of buffer spring D

Figure 10. effect of buffer spring for 1 MW convertor.

The dynamic response of an ocean current convertor of 700 kW power under Typhon irregular wave and current direction is investigated, as shown in Figure 11. The corresponding hydrodynamic coefficients and other parameters are determined based on the similarity law derived in Section 4.1 and listed in Appendix C, D. The parameters of the mooring system are listed in Table 4.

Table 4. the parameters of the system of 700kW convertor.

Parameter	Dimension	Parameter	Dimension
depth of seabed H_{bed}	1300m	length of rope A, L_A	5980m
length of rope B, L_B	152.97m	length of rope C, L_C	100m
length of rope D, L_D	70m	distance between two foundations, L_F	1196m
current velocity V	1.5m/s	net buonyance of invertor and platform F_{BNT}/ F_{BNB}	907.4/407.9tons
static drag of the invertor F_{DT}	103.9 tons	static drag of the platform F_{DB}	0.134 tons
mass of the platform M_1	463.0 tons	mass of the invertor M_2	1245.5 tons
mass of the pontoon 3, M_3	213.5tons	mass of the pontoon 4, M_4	277.8tons
cross-sectional area of surfaced cylinder of pontoon 3, A_{BX}	4.03m²	mass moment of inertia of the convertor about the x, y, z-axis, I_{Tx} / I_{Ty} / I_{Tz}	3.62×10^{11} / 1.10×10^{11} / 3.62×10^{11} $kg-m^2$
cross-sectional area of surfaced cylinder of pontoon 4, A_{BT}	4.03m²	mass moment of inertia of the platform about the x,y,z-axis, I_{Px} / I_{Py} / I_{Pz}	1.22×10^{9} / 2.03×10^{7} / 1.22×10^{9} $kg-m^2$
significant wave height H_s	15.4m	significant period T_p	16.5s

Preprints.org (www.preprints.org) | NOT PEER-REVIEWED | Posted: 24 July 2024 doi:10.20944/preprints202407.1940.v1

relative angle between current and wave a		30°	phase angles of six regular simulating the irregular wave φ_i	30/60/90/120/170 /300°
HMPE / Dyneema® SK75	Young's modulus E_{PE}	116GPa,	distance from gravities of platform and convertor	R_{TBx}=21.8m R_{TDy} =17.0m R_{TBz} = 21.8m $R_{PAx} = R_{PAy} = R_{PAz} = 6.6m$ $R_{PBx} = R_{PBz} = 7.7m$ $R_{PCy} = R_{PCz} = 3.3m$
	weight per unit length w_{PE}	17.16kg/m		
	diameter D_{PE}	149.7mm		
	cross sectional area A_{PE}	0.0176m²		
	fracture strength T_{frac}	1400tons		

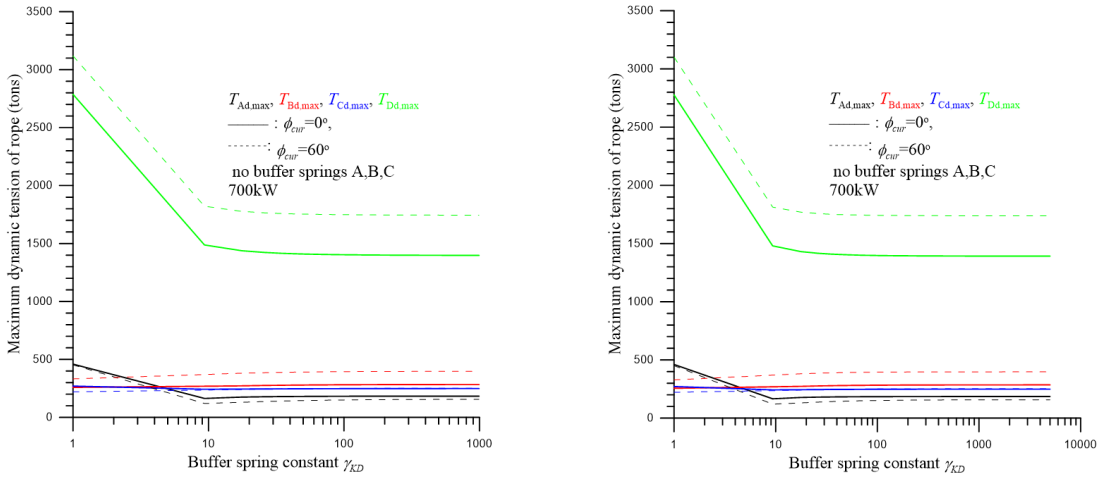

(a) $T_{j,frac}$=1400tons, j=A,B,C,D (b) $T_{j,frac}$=1400tons, j=A,B,C; $T_{D,frac}$=2000tons

Figure 11. effect of buffer spring for 700kW convertor.

Figure 11a demonstrates the effects of the buffer spring constant g_{KB} and the current direction φ_{cur} on the dynamic rope tensions of the pulley-rope system of 700 kW under typhoon irregular wave. The ropes A, B, C, and D have the same specification. The fracture strength $T_{j,frac}$=1400tons, j=A,B,C,D. It is found that if the buffer spring constant g_{KB}≅10, the dynamic tension $T_{Dd,max}$ is minimum and smaller than the fracture strength of rope T_{frac}=1400tons. When the buffer spring constant g_{KD}>100, i.e., the buffer spring D is not installed, the maximum dynamic tension $T_{Dd,max}$ (φ_{cur}=0°)=1394 tons, $T_{Dd,max}$ (φ_{cur}=60°)=1741 tons larger than the fracture strength 1400tons. To overcome this failure, only the specification of rope D is increased to $T_{D,frac}$=2000tons as listed in Table 3. As shown in Figure 11b, when the buffer spring constant g_{KD}>100, i.e., the buffer spring D is not installed, the maximum dynamic tension $T_{Dd,max}$ (φ_{cur}=0°)=1392 tons, $T_{Dd,max}$ (φ_{cur}=60°)=1738 tons smaller than the fracture strength 2000tons.

6. Conclusions

Preprints.org (www.preprints.org) | NOT PEER-REVIEWED | Posted: 24 July 2024 doi:10.20944/preprints202407.1940.v1

In this study, the similarity formulas of MW- and KW- level ocean convertor are constructed. According to these, the hydrodynamic damping and stiffness coefficients and other parameters of MW-level system can be determined. The novel pulley-main rope design for MW- level ocean convertor mooring system is proposed. Further, the mathematical dynamic model of a MW- level ocean convertor mooring system under irregular wave and current direction is derived. The analytical solution of this system is presented. The dynamic performance of the proposed 1 MW mooring system under irregular wave impact is investigated and discovered as follows:

1. The dynamic rope tensions $T_{Ad,max}$ and $T_{Bd,max}$ of the traditional single-traction rope system are larger than the fracture strength T_{frac}=2000tons. However, all the dynamic tensions of the pulley-rope system are smaller than the fracture strength. Obviously, the pulley-rope design can effectively reduce the dynamic rope tensions.

2. The dynamic responses of the above two kinds of mooring systems are different. The traditional single traction rope system is not affected by the flow direction, but the pulley-rope system is.

3. The static tension of rope A of the proposed system under the steady current only is close to half of the traditional single traction rope system.

4. For H_{bed} =1300m, if the rope length ratio, $4.1 \le r_{AH} \le 4.6$, all the dynamic tensions can be smaller than the fracture strength. For H_{bed} =1000m, if the rope length ratio, $4.0 \le r_{AH} \le 4.3$, all the dynamic tensions can be smaller than the fracture strength.

5. In a MW-level power generation system with the pulley-rope design, if buffer spring constant is very small, meanwhile the dynamic tension may become greater than the fracture strength. However, no buffer spring is set, it is reverse.

6. According to the theoretical analysis, the proposed MW-level ocean convertor mooring system with the pulley-rope design under typhoon wave impact is safety.

Acknowledgments: The support of GETRC from The Featured Areas Research Center Program within the framework of the Higher Education Sprout Project by MOE in Taiwan and the Ministry of Science and Technology of Taiwan, R. O. C. (NSTC 112-2218-E-110-008) are gratefully acknowledged.

Appendix A: Effective Masses of the Double Traction Sub-ropes $\{m_{eff,x}, m_{eff,y}, m_{eff,z}\}$

The effective masse $m_{eff,x}$ in the x-direction vibration:

As shown Figure 12, for the longitudinal vibration of the sub-ropes A_1 and A_2, the governing equation is

$$EA\frac{\partial^2 \chi_j}{\partial s_j^2} = \rho A \frac{\partial^2 \chi_j}{\partial t^2}, \quad s_j \in (0, L_{Aj}), \quad j = 1,\ 2 \tag{A1}$$

where χ_j is the dynamic displacement of the sub-rope A_1 and A_2.

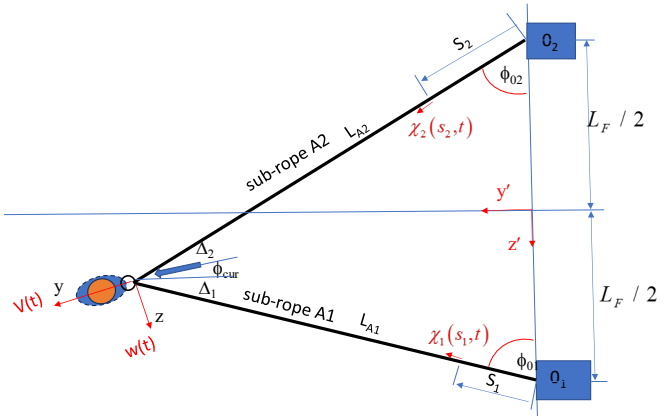

Figure 12. Top view of mooring system.

Preprints.org (www.preprints.org) | NOT PEER-REVIEWED | Posted: 24 July 2024 doi:10.20944/preprints202407.1940.v1

The boundary conditions are

$$\text{At } s_j=0: \quad \chi_j = 0 \qquad \text{(A2)}$$

$$\text{At } s_j=L_j: \quad M_1\ddot{u} + T_1 \sin\theta_{s1} + T_2 \sin\theta_{s2} = 0 \qquad \text{(A3)}$$

where u(t) is the dynamic x-direction displacement of platform. The relation between the displacement u and the elongation of the sub-ropes A_1 and A_2 is

$$u(t) = \chi_1\left(s_1 = L_{A1}, t\right)\sin\theta_{s1} = \chi_2\left(s_2 = L_{A2}, t\right)\sin\theta_{s2} \qquad \text{(A4)}$$

The dynamic tension of the sub-ropes A_1 and A_2

$$T_j = EA\frac{\partial\chi_j\left(L_{Aj}, t\right)}{\partial s_j}, j = 1,2 \qquad \text{(A5)}$$

Substituting Equations (A4-A5) into Equation (A3) and due to $T_1 = T_2$,

$$M_1\frac{\partial^2\chi_1\left(L_{A1}, t\right)}{\partial t^2}\sin\theta_{s1} + EA\frac{\partial\chi_1\left(s_1 = L_1, t\right)}{\partial s_1}\left(\sin\theta_{s1} + \sin\theta_{s2}\right) = 0 \qquad \text{(A6)}$$

The solution of Equation (A1) is assumed

$$\chi_j\left(s_j, t\right) = U_j(s_j)\sin\omega t \qquad \text{(A7)}$$

Substituting Equation (A7) into Equation (A1), one obtains

$$E\frac{d^2U_j}{ds_j^2} + \rho\omega^2 U_j = 0, \quad s_j \in \left(0, L_{Aj}\right) \qquad \text{(A8)}$$

The transformed boundary conditions are

$$\text{At } s_j=0: \quad U_j(0)=0 \qquad \text{(A9)}$$

$$\text{At } s_1=L_{A1}: \quad -\omega^2 M_1 U_1 \sin\theta_{s1} + EA\frac{dU_1}{ds_1}\left(\sin\theta_{s1} + \sin\theta_{s2}\right) = 0 \qquad \text{(A10)}$$

The fundamental solution of Equation (A8) is assumed

$$U_j(s_j) = e^{\lambda s_j} \qquad \text{(A11)}$$

Substituting Equation (A11) into Equation (A8),

$$\lambda_{1,2} = \pm j\sqrt{\frac{\rho}{E}}\omega \qquad \text{(A12)}$$

The general solution of Equation (A8) is

$$U_j(s_j) = d_1\cos\sqrt{\frac{\rho}{E}}\omega s_j + d_2\sin\sqrt{\frac{\rho}{E}}\omega s_j \qquad \text{(A13)}$$

Substituting (A13) into (A9), $d_1 = 0$. Substituting (A13) and (A14) into (A10), the frequency equation is obtained

$$\Omega\tan\Omega = \gamma_{mass,x} \qquad \text{(A14)}$$

where $\gamma_{mass,x} = \frac{\rho A L_{A1}}{M_1}\frac{\left(\sin\theta_{s1} + \sin\theta_{s2}\right)}{\sin\theta_{s1}}$. The dimensionless fundamental frequency

$$\Omega = \frac{\omega}{\left(\frac{1}{L_{A1}}\sqrt{\frac{E}{\rho}}\right)} \qquad \text{(A15)}$$

Via Equation (A14), one can determine the dimensionless frequency W.

The effective mass-spring model in the x-direction vibration is

$$\left(M_1 + m_{eff,x}\right)\ddot{u} + k_{eff,x}u = 0 \qquad \text{(A16)}$$

where $k_{eff,x} = \frac{EA}{L_A}\left(\frac{x_{01}}{L_{A1}} + \frac{x_{02}}{L_{A2}}\right)\left(\sin\theta_{s1} + \sin\theta_{s2}\right)$. The frequency of Equation (A16) is

 doi:10.20944/preprints202407.1940.v1

$$\omega = \sqrt{\frac{k_{eff,x}}{\left(M_1 + m_{eff,x}\right)}} \quad \text{(A17)}$$

Substituting Equation (A16) into Equation (A17), the effective mass in the x-direction motion is

$$m_{eff,x} = \frac{k_{eff,x}}{\Omega^2\left(\frac{1}{L_{A1}}\sqrt{\frac{E}{\rho}}\right)^2} - M_1 \quad \text{(A18)}$$

The effective masse $m_{eff,y}$ in the y-direction vibration:

In the similar way, the effective masse $m_{eff,y}$ in the y-direction vibration can be determined. The corresponding frequency equation is

$$\Omega \tan \Omega = \gamma_{mass,y} \quad \text{(A19)}$$

where $\gamma_{mass,y} = \frac{\rho A L_{A1}}{M_1} \frac{\left[\cos\theta_{s1}\cos\left(\Delta_1 + \phi_{cur}\right) + \cos\theta_{s2}\cos\left(\Delta_2\right)\right]}{\cos\theta_{s1}\cos\left(\Delta_1 + \phi_{cur}\right)}$. The dimensionless fundamental frequency W can be calculated via Equation (19). Further, the effective mass is

$$m_{eff,y} = \frac{k_{eff,y}}{\Omega^2\left(\frac{1}{L_{A1}}\sqrt{\frac{E}{\rho}}\right)^2} - M_1 \quad \text{(A20)}$$

where $k_{eff,y} = \frac{EA}{L_A}\left(\frac{y_{01}}{L_{A1}} + \frac{y_{02}}{L_{A2}}\right)\left(\cos\theta_{s1}\cos\left(\Delta_1 + \phi_{cur}\right) + \cos\theta_{s2}\cos\left(\Delta_2\right)\right)$.

The effective masse $m_{eff,z}$ in the z-direction vibration:

In the similar way, the effective masse $m_{eff,z}$ in the y-direction vibration can be determined. The corresponding frequency equation is

$$\Omega \tan \Omega = \gamma_{mass,z} \quad \text{(A21)}$$

where $\gamma_{mass,z} = \frac{\rho A L_{A1}}{M_1} \frac{\left[-\cos\theta_{s1}\sin\left(\Delta_1 + \phi_{cur}\right) + \cos\theta_{s2}\sin\left(\Delta_2\right)\right]}{\cos\theta_{s1}\sin\left(\Delta_1 + \phi_{cur}\right)}$. The dimensionless fundamental frequency W can be calculated via Equation (A21). Further, the effective mass is

$$m_{eff,z} = \frac{k_{eff,z}}{\Omega^2\left(\frac{1}{L_{A1}}\sqrt{\frac{E}{\rho}}\right)^2} - M_1 \quad \text{(A22)}$$

where $k_{eff,z} = \frac{EA}{L_A}\left(\frac{z_{01}}{L_{A1}} + \frac{z_{02}}{L_{A2}}\right)\left(-\cos\theta_{s1}\sin\left(\Delta_1 + \phi_{cur}\right) + \cos\theta_{s2}\sin\left(\Delta_2\right)\right)$.

Appendix B: Elements of the mass matrix $\mathbf{M} = \left[M_{i,j}\right]_{18\times 18}$

The translational inertia coefficients of platform 1:

$M_{1,1} = \left(M_1 + M_{eff,x}\right),\ M_{1,j} = 0, j \neq 1$; $M_{2,2} = \left(M_1 + M_{eff,y}\right), M_{2,j} = 0, j \neq 2$;

$M_{3,3} = \left(M_1 + M_{eff,z}\right), M_{3,j} = 0, j \neq 3$;

The translational inertia coefficients of invertor 2:

$M_{4,4} = M_2, M_{4,j} = 0, j \neq 4$; $M_{5,5} = M_2, M_{5,j} = 0, j \neq 5$; $M_{6,6} = M_2, M_{6,j} = 0, j \neq 6$;

The translational inertia coefficients of pontoon 3:

$M_{7,7} = M_3, M_{7,j} = 0, j \neq 7$; $M_{8,8} = M_3, M_{8,j} = 0, j \neq 8$; $M_{9,9} = M_3, M_{9,j} = 0, j \neq 9$;

The translational inertia coefficients of pontoon 4:

$M_{10,10} = M_4, M_{10,j} = 0, j \neq 10$; $M_{11,11} = M_4, M_{11,j} = 0, j \neq 11$; $M_{12,12} = M_4, M_{12,j} = 0, j \neq 12$

 doi:10.20944/preprints202407.1940.v1

The rotational inertia coefficients of invertor 2:

$M_{13,13}=I_{Tx}, M_{13,j}=0, j\neq 13$; $M_{14,14}=I_{Ty}, M_{14,j}=0, j\neq 14$; $M_{15,15}=I_{Tz}$, $M_{15,j}=0, j\neq 15$;

The rotational inertia coefficients of platform 1:

$M_{16,16}=I_{Px}$, $M_{16,j}=0, j\neq 16$; $M_{17,17}=I_{Py}$, $M_{17,j}=0, j\neq 17$; $M_{18,18}=I_{Pz}$, $M_{18,j}=0, j\neq 18$.

Appendix C: Elements of the Hydrodynamic Damping Matrix in similarity law $\mathbf{C}=\left[C_{i,j}\right]_{18\times 18}$

The translational hydrodynamic damping coefficients of platform 1:

$$C_{11}=-\frac{\partial f_{Px}}{\partial \dot{x}_{1d}}=5800\left(\frac{D_{P,pro}^2}{D_{P,\mathrm{mod}}^2}\right)(N-s/m),\qquad C_{12}=-\frac{\partial f_{Px}}{\partial \dot{y}_{1d}}=0,\qquad C_{13}=-\frac{\partial f_{Px}}{\partial \dot{z}_{1d}}=0,$$

$$C_{1,16}=-\frac{\partial f_{Px}}{\partial \dot{\varphi}_{1x}}=0,\qquad C_{1,17}=-\frac{\partial f_{Px}}{\partial \dot{\varphi}_{1y}}=0,\qquad C_{1,18}=-\frac{\partial f_{Px}}{\partial \dot{\varphi}_{1z}}=3.065\times 10^4\left[\frac{D_{P,pro}^2}{D_{P,mod}^2}\frac{\omega_{T,mod}}{\omega_{T,pro}}\right](N-s),$$

$C_{1j}=0, j\neq 1,2,3,16,17,18;$

$$C_{21}=-\frac{\partial f_{Py}}{\partial \dot{x}_{1d}}=121.4\left(\frac{D_{P,pro}^2}{D_{P,\mathrm{mod}}^2}\right)(N-s/m),\qquad C_{22}=-\frac{\partial f_{Py}}{\partial \dot{y}_{1d}}=768.4\left(\frac{D_{P,pro}^2}{D_{P,\mathrm{mod}}^2}\right)(N-s/m),$$

$$C_{23}=-\frac{\partial f_{Py}}{\partial \dot{z}_{1d}}=108.5\left(\frac{D_{P,pro}^2}{D_{P,\mathrm{mod}}^2}\right)(N-s/m),\qquad C_{2,16}=-\frac{\partial f_{Py}}{\partial \dot{\varphi}_{1x}}=7.375\times 10^4\left[\frac{D_{P,pro}^2}{D_{P,mod}^2}\frac{\omega_{T,mod}}{\omega_{T,pro}}\right](N-s),$$

$$C_{2,17}=-\frac{\partial f_{Py}}{\partial \dot{\varphi}_{1x}}=0,\quad C_{2,18}=-\frac{\partial f_{Py}}{\partial \dot{\varphi}_{1z}}=7.374\times 10^4\left[\frac{D_{P,pro}^2}{D_{P,mod}^2}\frac{\omega_{T,mod}}{\omega_{T,pro}}\right](N-s),$$

$C_{2j}=0, j\neq 1,2,3,16,17,18;$

$$C_{31}=-\frac{\partial f_{Pz}}{\partial \dot{x}_{1d}}=0,\qquad C_{32}=-\frac{\partial f_{Pz}}{\partial \dot{y}_{1d}}=0,\quad C_{33}=-\frac{\partial f_{Pz}}{\partial \dot{z}_{1d}}=5756\left(\frac{D_{P,pro}^2}{D_{P,\mathrm{mod}}^2}\right)(N-s/m),$$

$$C_{3,16}=-\frac{\partial f_{Pz}}{\partial \dot{\varphi}_{1x}}=-3.1174\times 10^4\left[\frac{D_{P,pro}^2}{D_{P,mod}^2}\frac{\omega_{T,mod}}{\omega_{T,pro}}\right](N-s),\quad C_{3,17}=-\frac{\partial f_{Pz}}{\partial \dot{\varphi}_{1y}}=0,$$

$$C_{3,18}=-\frac{\partial f_{Pz}}{\partial \dot{\varphi}_{1z}}=0,\quad C_{3j}=0, j\neq 1,2,3,16,17,18;$$

The translational hydrodynamic damping coefficients of invertor 2:

$$C_{44}=-\frac{\partial f_{Tx}}{\partial \dot{x}_{2d}}=1.465\times 10^6\left[\frac{D_{T,pro}^2}{D_{T,\mathrm{mod}}^2}\right](N-s/m),\quad C_{45}=-\frac{\partial f_{Tx}}{\partial \dot{y}_{2d}}=0,\quad C_{46}=-\frac{\partial f_{Tx}}{\partial \dot{z}_{2d}}=0,$$

$$C_{4,13}=-\frac{\partial f_{Tx}}{\partial \dot{\varphi}_{2x}}=0,\qquad C_{4,14}=-\frac{\partial f_{Tx}}{\partial \dot{\varphi}_{2y}}=0,\qquad C_{4,15}=-\frac{\partial f_{Tx}}{\partial \dot{\varphi}_{2z}}=0,$$

$C_{4j}=0, j\neq 4,5,6,13,14,15;$

$$C_{54}=-\frac{\partial f_{Ty}}{\partial \dot{x}_{2d}}=2.085\times 10^5\left[\frac{D_{T,pro}^2}{D_{T,\mathrm{mod}}^2}\right](N-s/m),\ C_{55}=-\frac{\partial f_{Ty}}{\partial \dot{y}_{2d}}=9.802\times 10^5\left[\frac{D_{T,pro}^2}{D_{T,\mathrm{mod}}^2}\right](N-s/m),$$

$$C_{56}=-\frac{\partial f_{Ty}}{\partial \dot{z}_{2d}}=1.256\times 10^5\left[\frac{D_{T,pro}^2}{D_{T,\mathrm{mod}}^2}\right](N-s/m),\quad C_{5,,13}=-\frac{\partial f_{Ty}}{\partial \dot{\varphi}_{2x}}=0,\quad C_{5,,14}=-\frac{\partial f_{Ty}}{\partial \dot{\varphi}_{2y}}=0,$$

$$C_{5,,15}=-\frac{\partial f_{Ty}}{\partial \dot{\varphi}_{2z}}=0,\qquad C_{5,j}=0, j\neq 4,5,6,13,14,15;$$

$$C_{64}=-\frac{\partial f_{Tz}}{\partial \dot{x}_{2d}}=0,\qquad C_{65}=-\frac{\partial f_{Tz}}{\partial \dot{y}_{2d}}=0,\quad C_{66}=-\frac{\partial f_{Tz}}{\partial \dot{z}_{2d}}=7\times 10^5\left[\frac{D_{T,pro}^2}{D_{T,\mathrm{mod}}^2}\right](N-s/m),$$

$$C_{6,13}=-\frac{\partial f_{Tz}}{\partial \dot{\varphi}_{2x}}=0,\qquad C_{6,14}=-\frac{\partial f_{Tz}}{\partial \dot{\varphi}_{2y}},\qquad C_{6,15}=-\frac{\partial f_{Tz}}{\partial \dot{\varphi}_{2z}}=0,$$

 doi:10.20944/preprints202407.1940.v1

$C_{6,j}=0, j\neq 4,5,6,13,14,15;$

The rotational hydrodynamic damping coefficients of convertor 2:

$$C_{13,4}=-\frac{\partial m_{Tx}}{\partial \dot{x}_{2d}}=0,\qquad C_{13,5}=-\frac{\partial m_{Tx}}{\partial \dot{y}_{2d}}=0,\qquad C_{13,6}=-\frac{\partial m_{Tx}}{\partial \dot{z}_{2d}}=-4.440\times10^{6}\left[\frac{D_{T,pro}^{3}}{D_{T,\mathrm{mod}}^{3}}\right](N-s),$$

$$C_{13,13}=-\frac{\partial m_{Tx}}{\partial \dot{\varphi}_{2x}}=13150\left[\frac{D_{T,pro}^{3}}{D_{T,\mathrm{mod}}^{3}}\frac{\omega_{T,\mathrm{mod}}}{\omega_{T,pro}}\right](N-m-s),\quad C_{13,14}=-\frac{\partial m_{Tx}}{\partial \dot{\varphi}_{2y}}=0,$$

$$C_{13,15}=-\frac{\partial m_{Tx}}{\partial \dot{\varphi}_{2z}}=0,\qquad C_{13,j}=0, j\neq 4,5,6,13,14,15;$$

$$C_{14,4}=-\frac{\partial m_{Ty}}{\partial \dot{x}_{2d}}=0,\qquad C_{14,5}=-\frac{\partial m_{Ty}}{\partial \dot{y}_{2d}}=0,\qquad C_{14,6}=-\frac{\partial m_{Ty}}{\partial \dot{z}_{2d}}=0,\qquad C_{14,13}=-\frac{\partial m_{Ty}}{\partial \dot{\varphi}_{2x}}=0,$$

$$C_{14,14}=-\frac{\partial m_{Ty}}{\partial \dot{\varphi}_{2y}}=2.837\times10^{8}\left[\frac{D_{T,pro}^{3}}{D_{T,\mathrm{mod}}^{3}}\frac{\omega_{T,\mathrm{mod}}}{\omega_{T,pro}}\right](N-m-s),$$

$$C_{14,15}=-\frac{\partial m_{Ty}}{\partial \dot{\varphi}_{2z}}=0,\ C_{14,j}=0, j\neq 4,5,6,13,14,15;$$

$$C_{15,4}=-\frac{\partial m_{Tz}}{\partial \dot{x}_{2d}}=7.453\times10^{6}\left[\frac{D_{T,pro}^{3}}{D_{T,\mathrm{mod}}^{3}}\right](N-s),\ C_{15,5}=-\frac{\partial m_{Tz}}{\partial \dot{y}_{2d}}=0,\qquad C_{15,6}=-\frac{\partial m_{Tz}}{\partial \dot{z}_{2d}}=0,$$

$$C_{15,13}=-\frac{\partial m_{Tz}}{\partial \dot{\varphi}_{2x}}=0,\quad C_{15,14}=-\frac{\partial m_{Tz}}{\partial \dot{\varphi}_{2y}}=0,$$

$$C_{15,15}=-\frac{\partial m_{Tz}}{\partial \dot{\varphi}_{2z}}=2.894\times10^{7}\left[\frac{D_{T,pro}^{3}}{D_{T,\mathrm{mod}}^{3}}\frac{\omega_{T,\mathrm{mod}}}{\omega_{T,pro}}\right](N-m-s),$$

$C_{15,j}=0, j\neq 4,5,6,13,14,15;$

The rotational hydrodynamic damping coefficients of platform 1:

$$C_{16,1}=-\frac{\partial m_{Px}}{\partial \dot{x}_{1d}}=0,\ C_{16,2}=-\frac{\partial m_{Px}}{\partial \dot{y}_{1d}}=0,\ C_{16,3}=-\frac{\partial m_{Px}}{\partial \dot{z}_{1d}}=8.671\times10^{4}\left[\frac{D_{P,pro}^{3}}{D_{P,\mathrm{mod}}^{3}}\right](N-s),$$

$$C_{16,16}=-\frac{\partial m_{Px}}{\partial \dot{\varphi}_{1x}}=1076\left[\frac{D_{P,pro}^{3}}{D_{P,\mathrm{mod}}^{3}}\frac{\omega_{T,\mathrm{mod}}}{\omega_{T,pro}}\right](N-m-s),\ C_{16,17}=-\frac{\partial m_{Px}}{\partial \dot{\varphi}_{1y}}=0,$$

$$C_{16,18}=-\frac{\partial m_{Px}}{\partial \varphi_{1z}}=0,\qquad C_{16,j}=0, j\neq 1,2,3,16,17,18;$$

$$C_{17,1}=-\frac{\partial m_{Py}}{\partial \dot{x}_{1d}}=0,\ C_{17,2}=-\frac{\partial m_{Py}}{\partial \dot{y}_{1d}}=0,\quad C_{17,3}=-\frac{\partial m_{Py}}{\partial \dot{z}_{1d}}=0,\qquad C_{17,16}=-\frac{\partial m_{Py}}{\partial \dot{\varphi}_{1x}}=0,$$

$$C_{17,17}=-\frac{\partial m_{Py}}{\partial \dot{\varphi}_{1y}}=0,\qquad C_{17,18}=-\frac{\partial m_{Py}}{\partial \dot{\varphi}_{1z}}=0,\qquad C_{17,j}=0, j\neq 1,2,3,16,17,18;$$

$$C_{18,1}=-\frac{\partial m_{Pz}}{\partial \dot{x}_{1d}}=8.654\times10^{4}\left[\frac{D_{P,pro}^{3}}{D_{P,\mathrm{mod}}^{3}}\right](N-s),\qquad C_{18,2}=-\frac{\partial m_{Pz}}{\partial \dot{y}_{1d}}=0,$$

$$C_{18,16}=-\frac{\partial m_{Pz}}{\partial \dot{\varphi}_{1x}}=0,\qquad C_{18,17}=-\frac{\partial m_{Pz}}{\partial \dot{\varphi}_{1y}}=0,$$

$$C_{18,18}=-\frac{\partial m_{Pz}}{\partial \dot{\varphi}_{1z}}=5.951\times10^{4}\left[\frac{D_{P,pro}^{3}}{D_{P,\mathrm{mod}}^{3}}\frac{\omega_{T,\mathrm{mod}}}{\omega_{T,pro}}\right](N-m-s),\quad C_{18,j}=0, j\neq 1,2,3,16,17,18;$$

Other coefficients: $C_{i,j}=0$, i=7, 8,..., 12, 17; $j=1,2,...,18$

The above coefficients were presented by Lin *et al.* [8].

Appendix D: Elements of the Stiffness Matrix in similarity law $\mathbf{K}=\left[K_{i,j}\right]_{18\times18}$

 doi:10.20944/preprints202407.1940.v1

The translational stiffness coefficients of platform 1:

$$K_{1,1}=\left[K_{Cd}+T_{As}\sum_{i=1}^{2}\left(\frac{\cos\theta_{Asi}}{L_{Ai}}\right)+K_{Ad}\varepsilon_{AX}\sum_{i=1}^{2}\sin\theta_{Ais}-\frac{T_{Bs}\cos\theta_{Bs}}{L_B}-K_{Bd}X_B\sin\theta_{Bs}\right],$$

$$K_{1,2}=K_{Ad}\varepsilon_{AY}-K_{Bd}Y_B\sin\theta_{Bs},\qquad K_{1,3}=K_{Ad}\varepsilon_{AZ}\sum_{i=1}^{2}\sin\theta_{Ais}-K_{Bd}Z_B\sin\theta_{Bs}$$

$$K_{1,4}=-\left(\frac{T_{Bs}\cos\theta_{Bs}}{L_B}-\sin\theta_{Bs}K_{Bd}\frac{(x_{2s}-x_{1s})}{L_B}\right),\quad K_{1,5}=-\sin\theta_{Bs}K_{Bd}\frac{(y_{2s}-y_{1s})}{L_B},$$

$$K_{1,6}=K_{Bd}Z_B\sin\theta_{Bs},\qquad K_{1,7}=K_{Cd},\qquad K_{1,16}=-\frac{\partial f_{Px}}{\partial\varphi_{px}}=0,\quad K_{1,17}=-\frac{\partial f_{Px}}{\partial\varphi_{py}}=0,$$

$$K_{1,18}=-\frac{\partial f_{Px}}{\partial\varphi_{pz}}=6508.5\left[\frac{D_{P,pro}^2}{D_{P,\mathrm{mod}}^2}\right](N),\qquad K_{1,j}=0,j\neq1,2,4,5,7,18;$$

$$\varepsilon_{AX}=\frac{(X_A-\varepsilon_{x01})}{r_{A1}}+\frac{(X_A-\varepsilon_{x02})}{r_{A2}},\varepsilon_{AY}=\frac{(Y_A-\varepsilon_{y01})}{r_{A1}}+\frac{(Y_A-\varepsilon_{y02})}{r_{A2}},\varepsilon_{AZ}=\frac{(Z_A-\varepsilon_{z01})}{r_{A1}}+\frac{(Z_A-\varepsilon_{z02})}{r_{A2}}$$

$$\varepsilon_{x01}=\frac{x_{01}}{L_A},\varepsilon_{y01}=\frac{y_{01}}{L_A},\varepsilon_{z01}=\frac{z_{01}}{L_A},\qquad \varepsilon_{x02}=\frac{x_{01}}{L_A},\varepsilon_{y02}=\frac{y_{01}}{L_A},\varepsilon_{z02}=\frac{z_{01}}{L_A},$$

$$r_{A1}=\frac{L_{A1}}{L_A},\ r_{A2}=\frac{L_{A2}}{L_A},\ X_A=\frac{x_{1s}}{L_A},\ Y_A=\frac{y_{1s}}{L_A},\ Z_A=\frac{z_{1s}}{L_A}$$

$$K_{2,1}=-\left(d_1+d_2K_{Ad}\varepsilon_{AX}-K_{Bd}X_B\cos\theta_{Bs}\right),\qquad K_{2,2}=-\left(d_2K_{Ad}\varepsilon_{AY}-K_{Bd}Y_B\cos\theta_{Bs}\right),$$

$$K_{2,3}=-\left(d_2K_{Ad}\varepsilon_{AZ}-K_{Bd}Z_B\cos\theta_{Bs}\right),\quad K_{2,4}=-\left(d_3+K_{Bd}X_B\cos\theta_{Bs}\right)$$

$$K_{2,5}=-K_{Bd}Y_B\cos\theta_{Bs},\qquad K_{2,6}=-K_{Bd}Z_B\cos\theta_{Bs}$$

$$K_{2,16}=-\frac{\partial f_{Py}}{\partial\varphi_{px}}=2072\left[\frac{D_{P,pro}^2}{D_{P,\mathrm{mod}}^2}\right]N,\quad K_{2,17}=-\frac{\partial f_{Py}}{\partial\varphi_{py}}=0,\quad K_{2,18}=-\frac{\partial f_{Py}}{\partial\varphi_{pz}}=2043.5\frac{N}{rad}$$

$$K_{2,j}=0,j\neq1\sim6,16\sim18$$

$$d_1=T_{As}\left[\frac{\sin\theta_{As1}\cos(\Delta_1+\phi_{cur})}{L_{A1}}+\frac{\sin\theta_{As2}\cos\Delta_2}{L_{A2}}\right]-\frac{T_{Bs}\sin\theta_{Bs}}{L_B},$$

$$d_2=-\left[\cos\theta_{As1}\cos(\Delta_1+\phi_{cur})+\cos\theta_{As2}\cos\Delta_2\right],\qquad d_3=-\frac{T_{Bs}\sin\theta_{Bs}}{L_B},$$

$$X_B=\frac{(x_{2s}-x_{1s})}{L_B},\quad Y_B=\frac{(y_{2s}-y_{1s})}{L_B},\quad Z_B=\frac{(z_{2s}-z_{1s})}{L_B}$$

$$\Delta_1=(\pi/2-\phi_{01}),\quad \Delta_2=(\pi/2-\phi_{02})-\phi_{cur}$$

$$K_{3,1}=\frac{T_{As}}{L_A}\left(\frac{\sin\theta_{As1}\sin(\Delta_1+\phi_{cur})}{r_{A1}}-\frac{\sin\theta_{As2}\sin\Delta_2}{r_{A2}}\right),\qquad K_{3,3}=\left(\frac{T_{Bs}}{L_B}+\frac{T_{Cs}}{L_C}\right),$$

$$K_{3,6}=-\frac{T_{Bs}}{L_B},\qquad K_{3,9}=-\frac{T_{Cs}}{L_C},\qquad K_{3,16}=-\frac{\partial f_{Pz}}{\partial\varphi_{px}}=-6547\left[\frac{D_{P,pro}^2}{D_{P,\mathrm{mod}}^2}\right]N,$$

$$K_{3,17}=-\frac{\partial f_{Pz}}{\partial\varphi_{py}}=0,\qquad K_{3,18}=-\frac{\partial f_{Pz}}{\partial\varphi_{pz}}=0,\qquad K_{3,j}=0,j\neq1,3,6,9,16.$$

The translational stiffness coefficients of convertor 2:

$$K_{4,1}=\left(\frac{T_{\mathrm{Bs}}\cos\theta_{Bs}}{L_B}+\sin\theta_{Bs}K_{Bd}\frac{(x_{2s}-x_{1s})}{L_B}\right),\quad K_{4,2}=\sin\theta_{Bs}K_{Bd}\frac{(y_{2s}-y_{1s})}{L_B},$$

$$K_{4,4}=\left(K_{Dd}-\frac{T_{\mathrm{Bs}}\cos\theta_{Bs}}{L_B}-\sin\theta_{Bs}K_{Bd}\frac{(x_{2s}-x_{1s})}{L_B}\right),\quad K_{4,5}=-\sin\theta_{Bs}K_{Bd}\frac{(y_{2s}-y_{1s})}{L_B},$$

$$K_{4,10}=-K_{Dd},\qquad K_{4,13}=-\frac{\partial f_{Tx}}{\partial\varphi_{Tx}}=0,\qquad K_{4,14}=-\frac{\partial f_{Tx}}{\partial\varphi_{Ty}}=0,$$

 doi:10.20944/preprints202407.1940.v1

$$K_{4,15}=-\frac{\partial f_{Tx}}{\partial \varphi_{Tz}}=1.5\times10^{6}\left[\frac{D_{T,pro}^{2}}{D_{T,\mathrm{mod}}^{2}}\right]N,\qquad K_{4,j}=0,\ j\neq1,2,4,5,10,15;$$

$$K_{5,1}=K_{Bd}\cos\theta_{B}\frac{x_{1s}-x_{2s}}{L_{B}},\quad K_{5,2}=K_{Bd}\cos\theta_{B}\frac{y_{1s}-y_{2s}}{L_{B}},\quad K_{53}=K_{Bd}\cos\theta_{B}\frac{z_{1s}-z_{2s}}{L_{B}},$$

$$K_{54}=-K_{51},\quad K_{55}=-K_{52},\quad K_{56}=-K_{53},\quad K_{5,13}=-\frac{\partial f_{Ty}}{\partial \varphi_{Tx}}=2.349\times10^{5}\left[\frac{D_{T,pro}^{2}}{D_{T,\mathrm{mod}}^{2}}\right]N,$$

$$K_{5,14}=-\frac{\partial f_{Ty}}{\partial \varphi_{Ty}}=0,\quad K_{5,15}=-\frac{\partial f_{Ty}}{\partial \varphi_{Tz}}=5.850\times10^{5}\left[\frac{D_{T,pro}^{2}}{D_{T,\mathrm{mod}}^{2}}\right]N,\quad K_{5,j}=0,\ j\neq1\sim6,13,15$$

$$K_{63}=-\frac{T_{Bs}}{L_{B}},\qquad K_{66}=\left(\frac{T_{Bs}}{L_{B}}+\frac{T_{Ds}}{L_{D}}\right),\qquad K_{6,12}=-\frac{T_{Ds}}{L_{D}},$$

$$K_{6,13}=-\frac{\partial f_{Tz}}{\partial \varphi_{Tx}}=-5.880\times10^{5}\left[\frac{D_{T,pro}^{2}}{D_{T,\mathrm{mod}}^{2}}\right]N,\quad K_{6,14}=-\frac{\partial f_{Tz}}{\partial \varphi_{Ty}}=0,\quad K_{6,15}=-\frac{\partial f_{Tz}}{\partial \varphi_{Tz}}=0$$

$$K_{6,j}=0,\ j\neq3,6,12,13$$

$$K_{6,3}=-\frac{T_{Bs}}{L_{B}},\qquad K_{6,6}=\left(\frac{T_{Bs}}{L_{B}}+\frac{T_{Ds}}{L_{D}}\right),\qquad K_{6,12}=-\frac{T_{Ds}}{L_{D}},$$

$$K_{6,13}=-\frac{\partial f_{Tz}}{\partial \varphi_{Tx}}=-5.880\times10^{5}\left[\frac{D_{T,pro}^{2}}{D_{T,\mathrm{mod}}^{2}}\right]N,\quad K_{6,14}=-\frac{\partial f_{Tz}}{\partial \varphi_{Ty}}=0,\ K_{6,15}=-\frac{\partial f_{Tz}}{\partial \varphi_{Tz}}=0$$

$$K_{6,j}=0,\ j\neq3,6,12,13;$$

The translational stiffness coefficients of pontoon 3:

$$K_{7,1}=-K_{Cd},\quad K_{7,7}=\left(K_{Cd}+A_{Bx}\rho g\right),\qquad K_{7,j}=0,\ j\neq1,7;$$

$$K_{8,2}=\frac{-T_{Cs}}{L_{C}},\quad K_{8,8}=\frac{T_{Cs}}{L_{C}},\qquad K_{8,j}=0,\ j\neq2,8\ ;$$

$$K_{9,3}=\frac{-T_{Cs}}{L_{C}},\ K_{9,9}=\frac{T_{Cs}}{L_{C}},\qquad K_{9,j}=0,\ j\neq3,9\ ;$$

The translational stiffness coefficients of pontoon 4:

$$K_{10,4}=-K_{\mathrm{D}d},\qquad K_{10,10}=K_{\mathrm{D}d}+A_{BT}\rho g,\quad K_{10,j}=0,\ j\neq4,10\ ;$$

$$K_{11,5}=\frac{-T_{Ds}}{L_{D}},\qquad K_{11,11}=\frac{T_{Ds}}{L_{D}},\qquad K_{11,j}=0,\ j\neq5,11;$$

$$K_{12,6}=\frac{-T_{Ds}}{L_{D}},\qquad K_{12,12}=\frac{T_{Ds}}{L_{D}},\qquad K_{12,j}=0,\ j\neq6,12;$$

The rotational stiffness coefficients of convertor 2:

$$K_{13,3}=\frac{-T_{Bs}R_{TBx}}{L_{B}},\qquad K_{13,6}=\frac{T_{Bs}R_{TBx}}{L_{B}},\qquad K_{13,13}=T_{Bs}\cos\theta_{Bs}R_{TBx}-\frac{\partial m_{Tx}}{\partial \varphi_{Tx}},$$

$$\frac{\partial m_{Tx}}{\partial \varphi_{Tx}}=4.866\times10^{6}\left[\frac{D_{T,pro}^{3}}{D_{T,\mathrm{mod}}^{3}}\right](N-m),\quad K_{13,14}=-\frac{\partial m_{Tx}}{\partial \varphi_{Ty}}=0,\qquad K_{13,15}=-\frac{\partial m_{Tx}}{\partial \varphi_{Tz}}=0,$$

$$K_{13,j}=0,\ j\neq3,6,13;$$

$$K_{14,6}=\frac{T_{Ds}R_{TDy}}{L_{D}},\qquad K_{14,12}=\frac{-T_{Ds}R_{TDy}}{L_{D}},\qquad K_{14,13}=-\frac{\partial m_{Ty}}{\partial \varphi_{Tx}}=-9.537\times10^{5}\left[\frac{D_{T,pro}^{3}}{D_{T,\mathrm{mod}}^{3}}\right](N-m)$$

$$K_{14,14}=T_{Ds}R_{TDy}-\frac{\partial m_{Ty}}{\partial \varphi_{Ty}}=T_{Ds}R_{TDy},\quad K_{14,15}=-\frac{\partial m_{Ty}}{\partial \varphi_{Tz}}=0,\quad K_{14,j}=0,\ j\neq6,12,13,14,15\ ;$$

$$K_{15,1}=\frac{-T_{Bs}R_{TBz}\cos\theta_{B}}{L_{B}},\ K_{15,4}=\frac{T_{Bs}R_{TBz}\cos\theta_{B}}{L_{B}},\ K_{15,13}=-\frac{\partial m_{Tz}}{\partial \varphi_{Tx}}=-5.022\times10^{4}\left[\frac{D_{T,pro}^{3}}{D_{T,\mathrm{mod}}^{3}}\right](N-m)$$

 doi:10.20944/preprints202407.1940.v1

$$K_{15,14}=-\frac{\partial m_{Tz}}{\partial \varphi_{Ty}}=0,\quad K_{15,15}=T_{Bs}R_{TBz}\cos\theta_B-\frac{\partial m_{Tz}}{\partial \varphi_{2z}},\quad \frac{\partial m_{Tz}}{\partial \varphi_{Tz}}=8.472\times10^6\left[\frac{D_{T,pro}^3}{D_{T,\mathrm{mod}}^3}\right](N-m),$$

$$K_{15,j}=0,\ j\neq 1,4,13\sim 15;$$

The rotational stiffness coefficients of platform 1:

$$K_{16,3}=\frac{T_{Bs}R_{PBx}}{L_B}-T_{As}R_{PAx}\left(\frac{1}{L_{A1}}+\frac{1}{L_{A2}}\right),\quad K_{16,6}=\frac{-T_{Bs}R_{PBx}}{L_B},$$

$$K_{16,16}=T_{As}R_{PAx}\left(\cos\theta_{A1s}+\cos\theta_{A2s}\right)+T_{Bs}\cos\theta_{Bs}R_{PBx}-\frac{\partial m_{Px}}{\partial \varphi_{px}},$$

$$\frac{\partial m_{Px}}{\partial \varphi_{px}}=1.038\times10^5\left[\frac{D_{P,pro}^3}{D_{P,\mathrm{mod}}^3}\right](N-m),\quad K_{16,17}=-\frac{\partial m_{Px}}{\partial \varphi_{Py}}=0,\quad K_{16,18}=-\frac{\partial m_{Px}}{\partial \varphi_{Pz}}=0,$$

$$K_{16,j}=0,\ j\neq 3,6,16\sim 18;$$

$$K_{17,3}=T_{As}R_{PAy}\left(\frac{1}{L_{A1}}+\frac{1}{L_{A2}}\right)+\frac{T_{Cs}R_{PCy}}{L_C},\quad K_{17,9}=\frac{-T_{Cs}R_{PCy}}{L_C},$$

$$K_{17,17}=T_{As}R_{PAy}\left(\cos\theta_{A1s}+\cos\theta_{A2s}\right)+T_{Cs}R_{PCy}-\frac{\partial m_{Py}}{\partial \varphi_{Py}}$$

$$\frac{\partial m_{Py}}{\partial \varphi_{Py}}=0,\qquad K_{17,16}=-\frac{\partial m_{Py}}{\partial \varphi_{px}}=0,\qquad K_{17,18}=-\frac{\partial m_{Py}}{\partial \varphi_{Pz}}=0,$$

$$K_{17,j}=0,\ j\neq 3,9,16\sim 18;$$

$$K_{18,1}=T_{As}R_{PAz}\left(\frac{\cos\theta_{A1s}}{L_{A1}}+\frac{\cos\theta_{A2s}}{L_{A2}}\right)-\frac{T_{Bs}\cos\theta_{Bs}R_{PBz}}{L_B},\qquad K_{18,2}=\frac{-T_{Cs}R_{PCz}}{L_C},$$

$$K_{18,4}=\frac{T_{Bs}\cos\theta_{Bs}R_{PBz}}{L_B},\qquad K_{18,5}=\frac{T_{Cs}R_{PBz}}{L_C},\qquad K_{18,16}=-\frac{\partial m_{Pz}}{\partial \varphi_{px}}=0,$$

$$K_{18,17}=-\frac{\partial m_{Pz}}{\partial \varphi_{Py}}=0,\ K_{18,18}=T_{As}R_{PAz}\left(\cos\theta_{A1s}+\cos\theta_{A2s}\right)+T_{Bs}\cos\theta_{Bs}R_{PBz}+T_{Cs}R_{PCz}-\frac{\partial m_{Pz}}{\partial \varphi_{Pz}},$$

$$\frac{\partial m_{Pz}}{\partial \varphi_{pz}}=1.010\times10^5\left[\frac{D_{P,pro}^3}{D_{P,\mathrm{mod}}^3}\right](N-m),\quad K_{18,j}=0,\ j\neq 1,2,4,5,16,17,18$$

Nomenclature

a_i	amplitude of the i^{th} regular wave
A_{BX}: A_{BT}	cross-sectional area of surfaced cylinder of pontoons 3 and 4, respectively
A_{BY}, A_{TY}	damping area of platform and convertor under current, respectively
C_{DFy}, C_{DTy}	damping coefficient of floating platform and convertor
E_i	Young's modulus of rope *i*, *i* = *A*, *B*, *C*, *D*
F_B	buoyance
f_p	significant frequency
f_{kj}	hydrodynamic force of element *k* in the *j*-direction
f_{Pys}, f_{Tys}	the drag of the floating platform and the convertor under steady current
H_{bed}	depth of seabed
H_s	significant wave height
I_{Tj}, I_{Pj}	mass moment of inertia of the convertor and the platform about the j-axis.
g	gravity
K_{id}	effective spring constant of rope *i*, E_iA_i/L_i
$\vec{K}_i$	wave vector of the *i*-th regular wave
L_i	length of rope *i*
L_E	horizontal distance between the convertor and platform, $\sqrt{L_B^2-(L_C-L_D)^2}$

 doi:10.20944/preprints202407.1940.v1

M_i	mass of element *i*
$M_{eff,i}$	effective mass of rope *A* in the *i*-direction
m_{ki}	hydrodynamic moment of convertor or platform about the *i*-axis
$\vec{R}$	coordinate
R_{TBx}	distance between the center of gravity of invertor and the rope *B*, about the x-axis.
R_{TDy}	distance between the center of gravity of invertor and the rope *D*, about the y-axis.
R_{TDy}	distance between the center of gravity of invertor and the rope *B*, about the z-axis
R_{PAx} , R_{PBx}	distances in the y-z plane from the center of gravity to the rope *A* and *B*, respectively
R_{PAy} , R_{PCy}	distances in the x-z plane from the center of gravity to the rope *A* and *C*, respectively
R_{PAz} , R_{PBz} , R_{PCZ}	distances in the x-y plane from the center of gravity to the ropes *A*, *B* and *C*, respectively
T_i	tension force of rope i
t	time variable
V	ocean current velocity
W_i	weight of component i
w_{PE}	weight per unit length of HMPE
x_i, y_i, z_i	displacements of component *i*
x_w	sea surface elevation
α	relative angle between the directions of wave and current
ρ	density of sea water
ω_T	angular speed of turbine
Ω	angular frequency of wave
φ_{kj}	angular displacement of convertor or platform about the *j*-axis
ϕ	phase delay of wave, $\phi = 2\pi L_E \cos\alpha / \lambda$
θ_i	angles of rope *i*
λ	length of wave
δ_i	elongation of rope *i*

Subscript:

0~4	mooring foundation, floating platform, convertor, and two pontoons, respectively
A, *B*, *C*, *D*	Ropes *A*, *B*, *C*, and *D*, respectively
mod	model
iα, *iβ*	component α, β of rope *i* = *A*, *B*, *C*, and *D*
frac	fracture
s, *d*	static and dynamic, respectively
PE	PE dyneema rope
P	platform
pro	ptototype
T	convertor

References

1. Chen, Y. Y.; Hsu, H. C.; Bai, C. Y., Yang Y., Lee C. W., Cheng H. K., Shyue S. W., Li M. S. Evaluation of test platform in the open sea and mounting test of KW Kuroshio power-generating pilot facilities. In Proceedings of the 2016 Taiwan Wind Energy Conference, Keelung, Taiwan, 24–25 November 2016.
2. IHI; NEDO. The demonstration experiment of the IHI ocean current turbine located off the coast of Kuchinoshima Island, Kagoshima Prefecture, Japan, 14 August 2017. Available online: https://tethys.pnnl.gov/project-sites/ihi-ocean-current-turbine (accessed on 28 August 2021).
3. Guo et al. Manufacture and sea trial of 20 kW Floating Kuroshio Turbine. (2021) NAMR110050; Ocean Affairs Council: Kaohsiung, Taiwan, 2021. (In Chinese)
4. Lin, S.M.; Chen, Y.Y.; Hsu, H.C.; Li, M.S. Dynamic Stability of an Ocean Current Turbine System. *J. Mar. Sci. Eng.* **2020**, *8*, 687; doi:10.3390/jmse8090687.

5. Lin, S.M.; Chen, Y.Y. Dynamic stability and protection design of a submarined floater platform avoiding Typhoon wave impact. *J. Mar. Sci. Eng.* **2021**, *9*, 977.
6. Lin, S.M.; Chen, Y.Y.; Liauh C.T. Dynamic stability of the coupled pontoon-ocean turbine-floater platform-rope system under harmonic wave excitation and steady ocean current. *J. Mar. Sci. Eng.* **2021**, *9*, 01425.
7. Lin S.M.; Liauh, C.T.; Utama, D.W. Design and dynamic stability analysis of a submersible ocean current generator-platform mooring system under typhoon irregular wave. *J. Mar. Sci. Eng.* **2022**, 10, 538.
8. Lin S.M., Utama D.W.; Liauh C.T. Coupled translational-rotational stability analysis of a submersible ocean current converter-platform mooring system under typhoon wave. *J. Mar. Sci. Eng.* **2023**, 11, 518. https://doi.org/10.3390/jmse11030518
9. Lin S.M., Wang W.R.and Yuan H. Transient translational-rotational motion of an ocean current converter mooring system with initial conditions. *J. Mar. Sci. Eng*. 2023, 11, 1533.
10. Pierson, W.J., Jr.; Moskowitz, L. A proposed spectral form for fully developed wind seas based on the similarity theory of S. A. Kitaigorodskii. J. Geophys. Res. Space Phys. 1964, 69, 5181–5190. https://doi.org/10.1029/jz069i024p05181.
11. Anagnostopoulos, S.A. Dynamic response of offshore platforms to extreme waves including fluid-structure interaction. Engineering Structures, 1982,4(3): 179-185.
12. Belibassakis, K. A. A boundary element method for the hydrodynamic analysis of floating bodies in variable bathymetry regions. Engineering analysis with boundary elements, 2008, 32(10): 796-810.
13. Geuzaine P.; Farhat C.; Brown G. Application of a three-field nonlinear fluid-structure formulation to the prediction of the aeroelastic parameters of an f-16 fighter. Computers and Fluids,2003, 32:3–29.
14. Bathe K.J.; Nitikitpaiboon C.; Wang X. A mixed displacement-based finite element formulation for acoustic fluid-structure interaction. Computers and Structures, 1995, 56(2-3):225–237.
15. Lin S.M.; Wang W. R.; Lee, S. Y.; Chen C. W.; Hsiao Y.C.; Teng M.J. Wave modes of a pre-stressed thick tube conveying blood on the viscoelastic foundation. Applied Mathematical Modelling, 2015, 39: 466–482.
16. Tsui,Y.Y.; Huang, Y.C.; Huang, C.L.; Lin, S.W. A finite-volume-based approach for dynamic fluid-structure interaction. Numerical Heat Transfer, Part B: Fundamentals, 2013, 64(4): 326-349.
17. Hasanpour, A.; Istrati, D.; Buckle, I. Coupled SPH–FEM Modeling of Tsunami-Borne Large Debris Flow and Impact on Coastal Structures. Journal of Marine Science and Engineering, 2021, 9(10), 1068. https://do.org/10.3390/jmse9101068
18. Shyue, S.W. Development and Promotion of Key Technologies of Ocean Current Energy; OAC108001; Ocean Affairs Council, Kaohsiung, Taiwan: 2019; pp. 4–103. (in Chinese)
19. Aggarwal, A.; Pákozdi, C.; Bihs, H.; Myrhaug, D.; Chella, M.A. Free Surface Reconstruction for Phase Accurate Irregular Wave Generation. *J. Mar. Sci. Eng.* 2018, 6, 105. https://doi.org/10.3390/jmse6030105.